Fetus-derived IGF2 matches placental development to fetal demand

Ionel Sandovici[1,2,3,*], Aikaterini Georgopoulou[1,3], Antonia S. Hufnagel[1], Samira N. Schiefer[1], Fátima Santos[3,4], Katharina Hoelle[1], Brian Y.H. Lam[2], Giles S.H. Yeo[2], Keith Burling[2], Jorge López-Tello[3], Moritz Reiterer[5,6], Abigail L. Fowden[3], Graham J. Burton[3], Amanda N. Sferruzzi-Perri[3], Cristina M. Branco[5,6] & Miguel Constância[1,2,3,*]

[1]Department of Obstetrics and Gynaecology and National Institute for Health Research Cambridge Biomedical Research Centre, Cambridge CB2 0SW, United Kingdom

[2]University of Cambridge Metabolic Research Laboratories and MRC Metabolic Diseases Unit, Institute of Metabolic Science, Addenbrookes Hospital, Cambridge CB2 0QQ

[3]Centre for Trophoblast Research, Department of Physiology, Development and Neuroscience, University of Cambridge, Cambridge CB2 3EG, United Kingdom

[4]Epigenetics Programme, Babraham Institute, Cambridge CB22 3AT, United Kingdom

[5]Physiological Laboratory, Department of Physiology, Development and Neuroscience, University of Cambridge, Cambridge CB2 3EG, United Kingdom

[6]Centre for Cancer research and Cell Biology, Queen's University Belfast, Belfast BT9 7AE, United Kingdom

*Correspondence to Ionel Sandovici (is299@cam.ac.uk) or Miguel Constância (jmasmc2@cam.ac.uk)

Abstract

Growth of a fetus is dependent upon the functional capacity of its placenta, but how the latter is matched to fetal demands is currently unknown. Critically, there is continuous expansion of the feto-placental microvasculature throughout pregnancy, along with morphogenic modifications in the overlying trophoblast epithelium. Here we demonstrate, through fetal and trophoblast specific genetic manipulations in the mouse, that signalling by IGF2 from the feto-placental endothelium and endocrine actions of circulating fetal IGF2 are required. We provide evidence that endothelial and fetal-derived IGF2 plays an important role in trophoblast morphogenesis, acting through *Gcm1* and *Synb*. The effects on placental microvasculature expansion are mediated through IGF2R and angiopoietin-Tie2/TEK signalling. Thus, our study reveals a direct role for IGF2-IGF2R axis on matching fetal demand to placental supply and establishes the principle that hormone-like signals from the fetus play important roles in the control of placental vascularization and trophoblast morphogenesis, findings that have potential clinical implications.

Main

The mammalian fetus is totally dependent upon the placenta for nutrients and oxygen. Little is known, however, about how placental functional capacity is matched to fetal demands. As gestation progresses, the increase in fetal size requires a higher level of demand for nutrients and consequently a higher level of supply. Depending on the species, the surface area for nutrient exchange increases 5 to 15 fold between mid and late gestation[1]. This remarkable adaptation is likely to occur, at least in part, in response to fetus-derived signals of demand, but this important principle remains untested.

We have proposed that imprinted genes, in particular *Igf2*, play central roles in controlling both the fetal demand for, and the placental supply of, maternal nutrients[2,3,4]. The *Igf2* (insulin-like growth factor 2) gene encodes a small polypeptide that is highly abundant in both fetal tissues and fetal circulation. It is one of the most potent growth factors during intrauterine development, affecting the metabolism, proliferation, survival and differentiation of a wide variety of cell types[5,6,7,8]. In humans, reduced *Igf2* expression contributes to the intra-uterine growth restriction in patients with Silver-Russell syndrome (SRS)[9]. Conversely, bialellic *Igf2* expression caused by loss of *Igf2* imprinting is observed in Beckwith-Wiedemann patients (BWS), a syndrome characterized by somatic overgrowth and increased predisposition to tumours[9]. IGF2 exerts its effects by binding to several IGF/INS receptors (IGF1R, INSR, IGF1/INSR hybrids, IGF2R)[10,11]. IGF2 binds to IGF2R with the highest affinity, which leads to either IGF2 degradation in the lysosomes or signalling via G-proteins[10,12,13].

Here, we apply novel genetic approaches to define the signalling mechanisms of demand to the placenta by creating mouse models with a growth mismatch between the placenta and the fetus, using genetic manipulations of the IGF system. We first show that circulating IGF2 levels increase in late gestation, thus reflecting fetal size and higher demand. Decreasing the demand by lowering IGF2 levels in both the fetus and circulation abolishes the capacity of the placenta to increase the surface area in late gestation; conversely, increased demand by excess fetal IGF2 has the opposite effect. Mechanistically, we show that fetus-derived and circulating IGF2 signalling is essential for the appropriate growth of the fetal-derived vasculature and the underlying trophoblast. These effects are mediated in part by IGF2-IGF2R signalling in the feto-placental vascular endothelium. Our work demonstrates that the interaction of circulating IGF2 and endothelial IGF2 with the trophoblast is essential for matching the placental surface area for nutrient exchange (supply) to the growth rate of fetal tissues (demand).

Expansion of placental labyrinth coincides with elevated levels of circulating and endothelial IGF2

The gas and nutrient exchange layer of the mouse placenta (labyrinthine zone – Lz) increased in size with gestational age (Fig. 1a), matching the fetal weight (Fig. 1b). Concomitantly, fetal plasma IGF2 increased approximately two-fold between E16 and E19 (Fig. 1c). At these two developmental stages, we also observed a significant and positive correlation between fetal plasma IGF2 and fetal weights (Fig. 1d). Within the placental Lz, *Igf2* expression was the highest in feto-placental endothelial cells (FPEC) (Fig. 1e) and its mRNA levels increased approximately six-fold between E14 and E19 (Fig. 1f). *Igf2* ranked as the highest expressed gene in FPEC RNA-Seq transcriptome at E16, and several other known imprinted genes[14] ranked in the top one hundred out of approximately 14,000 genes detected (Fig. 1g and Supplementary Table 1). IGF2 protein was also highly expressed in FPEC (Fig. 1h), and significantly higher than in the surrounding trophoblast cells (Fig. 1i).

Fetal and endothelial IGF2 control placental labyrinthine expansion

To explore whether fetus-derived IGF2 plays a direct role in placental development, we first used a conditional allele ($Igf2^{+/fl}$) to delete *Igf2* in the epiblast lineage using the $Meox2^{Cre}$ line[15] (Fig. 2a and Extended Data Fig. 1). The deletion of *Igf2* from embryonic organs and FPEC, but not extra-embryonic tissues, led to placental growth restriction from E14 onwards (Fig. 2b). Stereological analyses indicated that only the placental compartments containing embryonic-derived structures (i.e. Lz and the chorionic plate – Cp) were smaller in the $Meox2^{Cre/+}$; $Igf2^{+/fl}$ mutants (referred subsequently as $Igf2^{EpiKO}$) (Fig. 2c). The continuous expansion of the Lz, measured as volume increase, that occurs in late gestation between E14 and E19 was severely compromised in mutants (Fig. 2c). The overall volume, surface area and total length of fetal capillaries (FC) were normal at E14, but became abnormal from E16 onwards (Fig. 2d and Extended Data Fig. 2a). Notably, all other components of placental Lz, not

86 originating from the embryonic lineage, (i.e. labyrinthine trophoblast – LT, and maternal blood spaces
87 – MBS) were also reduced in volume, to a similar extent as the FC (Fig. 2d). These findings provide
88 evidence for a role of fetus-derived IGF2 on the expansion of placental Lz in late gestation.

89 IGF2 is highly expressed in FPEC as previously shown in Fig. 1e-i. Therefore, we next tested whether
90 endothelial-derived IGF2 plays a role in placental development. *Igf2* deletion in the fetal endothelium,
91 including FPEC, using the *Tek*^{Cre} line[16] (Fig. 2e and Extended Data Fig. 3) led to a moderate but
92 significant fetal and placental growth restriction, evident from E16 onwards (Fig. 2f). Mutant *Tek*$^{Cre/+}$;
93 *Igf2*$^{+/fl}$ (referred subsequently as *Igf2*^{ECKO}) placentae had reduced volumes of Cp and Lz at both E16 and
94 E19 (Fig 2g), but less striking when compared to *Igf2*^{EpiKO} mutants (Fig. 2c). Within the Lz, the LT was
95 reduced at both E16 and E19, while the MBS and FC were comparable to controls at E16, but
96 significantly reduced at E19 (Fig. 2h and Extended Data Fig. 2b).

97 We conclude that the 'small' labyrinthine phenotype observed in *Igf2*^{EpiKO} mutants is more severe than
98 in *Igf2*^{ECKO} mutants, which suggests that full placental Lz expansion in late gestation requires both
99 fetus-derived and endothelial-derived IGF2.

100 **Fetus-derived IGF2 is essential for placental morphogenesis and microvasculature expansion**

101 To uncover the molecular mechanisms responsible for the placental Lz expansion, we first performed
102 microarray analysis in micro-dissected Lz samples from E19 *Igf2*^{EpiKO} mutants and controls.
103 Differentially expressed genes (DEG) were enriched in genes implicated in vasculature development
104 and immune responses (Fig. 3a and Extended Data Fig. 4a,b). We identified a classic molecular
105 signature of impaired angiogenesis – reduced angiopoietin-Tie2/TEK signalling[17] (Fig. 3b and
106 Supplementary Table 2). Lower levels of *Angpt1* and *Tek*, and increased expression of *Angpt2* were
107 validated by qRT-PCR in an independent set of biological samples in late gestation (Fig. 3b). Consistent
108 with the well-established roles of the angiopoietin-Tie2/TEK signalling in the control of endothelial cell
109 survival and proliferation[17], placental TUNEL staining revealed a six-fold increase in apoptotic cell
110 frequency in mutants at E16, specifically in the Lz (Fig. 3c). CD31-stained (marking endothelial cells) or
111 methylene blue-stained resin sections revealed the presence of feto-placental capillaries lacking
112 endothelial cells, or obstructed and thrombotic capillaries surrounded by highly disorganized and
113 fragmented endothelial cells (Fig. 3d). These observations indicate that a large proportion of the
114 apoptotic cells are FPEC. Furthermore, endothelial cell proliferation measured by flow cytometry was
115 significantly reduced at E16 (Fig. 3e and Extended Data Fig. 4c), and this finding was confirmed by
116 immunofluorescence (Extended Data Fig. 4d).

117 In addition to vascular pathways, the expression microarrays also identified transcriptional
118 upregulation of genes related to immune responses and leukocyte migration (Fig. 3a). Among these
119 was *Adgre1*, a gene that encodes the glycoprotein F4/80, a highly specific cell-surface marker for
120 murine macrophages[18]. The up-regulation of *Adgre1* was confirmed by qRT-PCR in placental Lz also at
121 E16–(Fig. 3f). Immunostaining for F4/80 showed that the total number of macrophages in Lz was
122 significantly higher in mutants than controls (Fig. 3f). Additionally, clusters of macrophages
123 surrounding feto-placental capillaries were found exclusively in mutants (Fig. 3g). Next, we assessed
124 the impact of the described increased cell death, reduced cell proliferation and macrophage
125 infiltration, on capillary remodelling across gestation by CD31 immunostaining. The density of FC was
126 dramatically reduced at E16 and E19, suggestive of a disproportionate loss of FPEC (Fig. 3h).

127 Importantly, the array data indicated downregulation of key genes involved in syncytiotrophoblast
128 differentiation (*i.e. Gcm1* and *Synb* – which are expressed specifically in layer II of the
129 syncytiotrophoblast, SynT-II, which is closest to FC; see Supplementary Table 2). To validate these

130 observations, we performed qRT-PCR for, and confirmed significant transcriptional reductions of,
131 SynT-II-specific genes[19,20] *Gcm1*, *Synb* and *Slc16a3* (Fig. 3i). However, only the SynT-I specific[19,20,21]
132 gene *Slc16a1* was modestly down-regulated, but not *Ly6e* and *Syna* (Extended Data Fig. 4e).

133 Together, our data show that lack of fetus-derived IGF2 triggers dysregulation of angiopoietin-
134 Tie2/TEK signalling in late gestation, with consequent reduced FPEC proliferation and excessive cell
135 death with associated placental macrophage infiltration. It also highlights that fetus-derived IGF2
136 supports normal development of the trophoblast cells, particularly the SynT-II layer, in a
137 paracrine/endocrine manner, with a knock-on effect on the development of maternal blood spaces.

138 **Endocrine IGF2 is a fetus-derived signal that matches placental supply to fetal demand**

139 To provide further insights into the roles of fetus-derived IGF2 in matching supply to fetal demand we
140 analysed five genetic models with either deletion of *Igf2* in fetal tissues, endothelium, trophoblast or
141 ubiquitously, or overexpression of *Igf2* in fetal tissues (Fig. 4). For these models we used flow
142 cytometry to count FPEC (defined as $CD31^+/CD41^-$ cells[22]) and measured labyrinthine weight and
143 circulating IGF2 levels. In $Igf2^{EpiKO}$ mutants, as expected from the immunostainings shown in Fig. 3h,
144 we observed a severe deficit in the total number and the proportion of FPEC at E16 and E19, but
145 normal values at E14 (Fig. 4a). The linear Lz expansion expected with gestational age was not observed
146 in this model, matching the severe reductions in FPEC numbers and circulating IGF2 (Fig. 4a). In
147 contrast, in $Igf2^{ECKO}$ mutants lacking endothelial *Igf2*, circulating levels of IGF2 were only moderately
148 reduced and total numbers of FPEC, but not relative numbers, were only significantly reduced at E19
149 (Fig. 4b). Lz expansion in this model was only blunted at the end of gestation (Fig. 4b). A deletion of
150 *Igf2* specifically in the trophoblast cells of the placenta using $Cyp19^{Cre}$ ($Igf2^{+/fl}$; $Cyp^{Cre/+}$ referred
151 subsequently as $Igf2^{TrKO}$)[23] (Fig. 4c and Extended Data Fig. 5a-e) did not result in changes in FPEC
152 numbers and circulating IGF2, demonstrating that FPEC expansion is independent of trophoblast-
153 derived IGF2. Consequently, Lz expansion was normal in this model (Fig. 4c). Ubiquitous deletion of
154 *Igf2* in embryo and trophoblast using CMV^{Cre} ($Igf2^{+/fl}$; $CMV^{Cre/+}$ referred subsequently as $Igf2^{UbKO}$)[24] (Fig.
155 4d and Extended Data Fig. 5f) led to a loss of FPEC similar to that observed in the $Igf2^{EpiKO}$ mutants,
156 further demonstrating that trophoblast-derived IGF2 does not contribute significantly to FPEC
157 expansion. Lz weight was severely reduced from E14, in line with the near complete absence of IGF2
158 in fetal circulation (Fig. 4d). Conversely, reactivating the transcriptionally silent maternal *Igf2* allele in
159 $H19DMD^{fl/+}$; $Meox2^{+/Cre}$ mutants[25] (referred subsequently as *H19*-DMD^{EpiKO}) (Fig. 4e and Extended Data
160 Fig. 5g,h), which led to increased levels of circulating IGF2, was associated with an increase of Lz weight
161 and higher numbers of FPEC at E16 and E19 (Fig. 4e).

162 Taken together, these results show that IGF2 produced by fetal organs and secreted into the fetal
163 circulation stimulates the expansion of placental Lz, matching FPEC numbers to the fetal demand.

164 **IGF2 signalling controls expression of FPEC-derived angiogenic factors**

165 We hypothesised that the interaction of circulating IGF2 and the trophoblast, via FPEC, are key events
166 underlying the feto-placental microvascular remodelling. To establish the molecular signatures of IGF2
167 effects on FPEC we carried out RNA-Seq analysis on FACS-isolated endothelial cells from E16 placental
168 Lz of $Igf2^{EpiKO}$ mutants and controls (Fig. 5 and Extended Data Fig. 6). Gene ontology (GO) analysis of
169 DEGs showed statistical enrichment of biological processes related to immune responses, cell
170 migration, impaired cell proliferation and angiogenesis, extracellular matrix organization and response
171 to hypoxia (Fig. 5a,b and Supplementary Table 3). We validated representative DEGs using qRT-PCR in
172 independent biological samples, including genes encoding proteins secreted by the endothelial cells
173 into the extracellular space that have known anti-angiogenic effects (*Angpt2*[17], *Adamts1*[26], *Cxcl10*[27],

174 *Thbs1*[28]), factors implicated in cell migration and response to hypoxia (*Edn1*[29]), an interferon-response
175 gene (Iigp1[30]), an inhibitor of cell proliferation (*Cdkn1a*[31]) and a regulator of embryonic vascular
176 development (*Hey2*[32]) (Fig. 5c). Next, we searched for transcription factor (TF) binding motifs enriched
177 within the promoters of all DEGs. This analysis identified significant enrichments for binding sites of
178 four TF encoded by DEGs – KLF4, EGR1, IRF7 and HEY2 (Fig. 5d and Supplementary Table 3).
179 Significantly, the four TFs control the expression of several proteins involved in angiogenesis (labelled
180 with * in Fig. 5e and further presented in Supplementary Table 4), some of which are secreted by the
181 endothelial cells into the extracellular space (Supplementary Table 4). This analysis also highlighted
182 several chemokines that were up-regulated in FPEC (such as CCL2[33] and IL15[34]) that are likely involved
183 in attracting and modulating the activity of macrophages that surround the feto-placental capillaries
184 (as shown in Fig. 3g). Thus, we established that IGF2 signalling is necessary for proliferation and
185 survival of FPEC and modulates their angiogenic properties.

186 **IGF2 signalling on FPEC is independent of IGF1R and is mediated by IGF2R *in vitro* and *in vivo***

187 To further investigate the role of IGF2 in fetal capillary remodelling and identify the receptors that
188 might mediate its effects on endothelial cells, we isolated primary FPEC from E16 wild-type placental
189 Lz and cultured them *ex vivo* (Extended Data Fig. 7a-c). Only the type I (*Igf1r*) and type II (*Igf2r*)
190 receptors were expressed in FPEC both *in vivo* and *ex vivo* (Fig. 6a,b and Extended Data Fig. 7d).
191 Exposure of cultured FPEC, which express low levels of *Igf2*, to exogenous IGF2 significantly increased
192 their ability to form capillary-like tube structures when seeded on matrigel (Extended Data Fig. 7e and
193 Fig. 6c), demonstrating that IGF2 exerts direct angiogenic effects on FPEC. We also exposed cultured
194 FPEC to IGF2^{Leu27}, an analogue previously shown to bind to IGF2R with high selectivity[35], which
195 stimulated capillary-like tube formation although to a lesser extent compared to IGF2 (Fig. 6b,c). When
196 FPEC were treated with IGF2 and picropodophyllin (PPP), a small molecule that inhibits
197 phosphorylation of IGF1R without interfering with INSR activity[36], their ability to form capillary-like
198 tube structures was very similar to that of cells treated with IGF2 alone (Fig. 6b,c). Thus, IGF2 exerts
199 direct angiogenic effects on primary FPEC, which are mediated by IGF2R and are independent of
200 IGF1R.

201 We further confirmed these *in vitro* findings by knocking-out these receptors (IGF1R and IGF2R) *in*
202 *vivo*. Accordingly, efficient deletion of *Igf1r* from the endothelium (*Igf1r*^{ECKO}) did not have any
203 significant impact on fetal, whole placenta or placental Lz growth kinetics, nor did it alter the total and
204 relative numbers of FPEC/Lz, apart from a slight increase in the percentage of FPEC at E19 (Extended
205 Data Fig. 8a-e). Strikingly, the deletion of *Igf2r* from the endothelium (*Igf2r*^{ECKO} – Extended Data Fig.
206 8f,g) resulted in a reduction in the percentage of FPEC/placental Lz at both E16 and E19, further
207 confirmed by a reduced density of CD31^{+} cells by immunofluorescent staining (Fig. (Fig. 6d, e). The
208 total number of FPEC/Lz was also significantly reduced at E16, but became normal at E19 (Fig. 6d),
209 with Lz being overgrown from E16 onwards (Fig. 6f) coincident with an increase in levels of circulating
210 IGF2 in plasma (Fig. 6g). Together, our *in vitro* and *in vivo* experiments demonstrate that IGF2R
211 mediates, at least partially, the signalling actions of IGF2 on FPEC.

212

213 **Discussion**

214

215 The major finding of this study is the demonstration that fetal growth demand signals are major
216 regulators of placental development and function. Although a vast number of genetic pathways have
217 been discovered that are important for the development of different cell types in the placenta and
218 the fetus, there are no functional genetic investigations to date on how the fetus signals demand to

219 the placenta and how the placenta matches the fetal demands. We tackled these questions with an
220 innovative experimental design, which is based on the manipulation of the growth rate of fetal tissues
221 independent of the placenta, and vice-versa, in the mouse. We used conditional targeting of imprinted
222 genes with well-established growth functions (*Igf2*, *Igf2r*, *H19*) as model systems (importantly, due to
223 imprinting, the mother is phenotypically normal). The analysis of these models of mismatch between
224 supply and demand allowed us to establish a number of key mechanistic principles that regulate the
225 cooperative signalling between the fetus and the placenta and, consequently, the control of maternal
226 resources.

227 Firstly, we found that circulating IGF2 correlates positively with fetal size in late gestation, reflecting
228 the growth rate of fetal tissues and the demand for nutrients. Mice with a severe decrease in levels of
229 circulating/fetal IGF2, and thus fetal demand, showed a drastic (and disproportionate) loss of feto-
230 placental endothelial cells. This severe placental angiogenesis phenotype was associated with reduced
231 endothelial cell proliferation and increased apoptosis, altered differentiation of the overlying
232 trophoblast and reduced density of maternal blood spaces, ultimately leading to a failure in the
233 expansion of the labyrinthine layer and surface area for nutrient transport. Conversely, increased
234 demand for nutrients caused by bi-allelic *Igf2* expression, which drove higher growth rates, led to
235 'overexpansion' of the labyrinthine layer. Secondly, we also found that feto-placental endothelial cells
236 are a significant source of IGF2, with levels increasing with gestational age. Endothelial *Igf2*-deficient
237 mice show modest reductions in circulating IGF2 and impaired expansion of the microvasculature and
238 labyrinthine layer, but no disproportionate reduction in number of placental endothelial cells (which
239 is only seen when circulating IGF2 is severely reduced). These findings establish the important
240 principle that hormone-like signals from the fetus, such as IGF2, are required for the normal expansion
241 of the labyrinthine layer and surface area of the placenta.

242 Based on the experimental evidence provided in this study, we propose a model (Fig. 6h) in which
243 fetus-derived IGF2 is the signal that allows matching placental supply capacity to fetal demand. At the
244 placenta interface, circulating IGF2 directly stimulates endothelial cell proliferation and survival, and
245 capillary branching through IGF2R (as shown *in vivo* and *ex-vivo*). Circulating IGF2 may also directly
246 control the growth and differentiation of the underlying trophoblast, as it can cross (in free form or in
247 binary complexes) the capillary walls or permeate through the fenestrated endothelium[37]. We suggest
248 that the feto-placental endothelium is a large reservoir of IGF2, boosting further IGF2 signalling, and
249 acting in a paracrine and autocrine manner to control the growth and remodelling of fetal capillaries,
250 and trophoblast morphogenesis. Importantly, the effect of IGF2 signalling on feto-placental
251 microvascular remodelling seems specifically driven by fetus-derived IGF2. Accordingly, we did not
252 find any evidence that IGF2 produced by the trophoblast has a direct role on vascularization, being
253 instead required for trophoblast morphogenesis. We therefore suggest that the key role of circulating
254 IGF2 is to provide fetus-derived angiogenic signals to promote the vascular tree expansion in later
255 gestation, in conjunction with local IGF2, derived from the fetal endothelium of the placenta.
256 Mechanistically, the most likely molecular effectors of fetus-derived IGF2 signalling on
257 microvasculature expansion and trophoblast morphogenesis are the angiopoietin-Tie2/TEK signalling
258 and the key trophoblast differentiation genes *Gcm1* and *Synb*, respectively.

259 Our study has a number of important implications. It provides insights into the complex interplay
260 between trophoblast branching morphogenesis and placental vascularization. To our knowledge, IGF2
261 is the first example of a hormone-like molecule that signals fetal demand to the placenta by adapting
262 the expansion of feto-placental microvasculature and trophoblast morphogenesis to the embryo size.
263 Matching placental supply to fetal demand also involves IGF2R – the other imprinted member of the
264 IGF family[38]. The imprinting of the IGF system is thus likely to have played a key evolutionary role in

265 the origins of the expansion of the feto-placental microvasculature and surface area for nutrient
266 transport throughout pregnancy – a fundamental biological process that is observed in all eutherian
267 species[1]. In humans, circulating levels of IGF2 in the umbilical cord progressively increase between 29
268 weeks of gestation and term, similarly to our findings in the mouse[39]. Additionally, large-for-
269 gestational age and small-for-gestational age babies, have been reported to show increased and
270 reduced levels of IGF2 in the umbilical cord, respectively[40,41]. Moreover, placentae obtained from
271 imprinting growth syndrome patients with disrupted IGF2 signalling are often associated with
272 placentomegaly in BWS cases, due to hypervascularization and hyperplasia[42,43] and small hypoplastic
273 placentas in SRS cases[44], showing striking similarities to our mouse studies. Importantly, most cases
274 of poor placentation in FGR (fetal growth restriction) reported so far were related to placental
275 malperfusion from the maternal side and in response to a perturbed maternal environment[45]. Our
276 findings suggest that poor placentation in humans could be caused by deficient microvasculature
277 expansion due to reduced fetus-derived IGF2 signalling, with important clinical implications.

278

279 **Methods**

280 **Mice**

281 Mice were bred, maintained and mated under pathogen-free conditions at the University of
282 Cambridge Phenomics Unit (West Forvie), in accordance with the University of Cambridge Animal
283 Welfare and Ethical Review Body and the United Kingdom Home Office Regulations. The morning of
284 the copulation plug discovery was counted as embryonic day 1 (E1).

285 The *Igf2*$^{fl/fl}$ mice were generated in our laboratory[46]. *Meox2*^{Cre} mice[15], *Tek*^{Cre} mice[16], *Cyp19*^{Cre} mice[23],
286 *CMV*^{Cre} mice[24] and *Igf1r*$^{fl/fl}$ mice[47] were imported from the Jackson Laboratory (Maine, USA). *Meox2*^{Cre}
287 is active starting at E5 in the epiblast, which gives rise to the entire embryo proper and FPEC[15]. *Tek*^{Cre}
288 (also known as *Tie2*^{Cre}) activity starts at E7.5 in the endothelial cell lineage, including FPEC[16]. *Cyp19*^{Cre}
289 is active from E6.5 in the early diploid trophoblast cells that give rise to spongiotrophoblast, giant cells,
290 and labyrinthine trophoblast cells[23]. *CMV*^{Cre} activity starts soon after fertilization and induces
291 ubiquitous deletion of floxed alleles in all tissues, including the germline[24]. *Rosa26* ^{fl}STOP^{fl}YFP mice[48]
292 were kindly provided by Dr. Martin Turner (The Babraham Institute, Cambridge), Ai9(RCL-tdT) mice[49]
293 by Prof. William Colledge (University of Cambridge), *H19*-DMD$^{fl/fl}$ mice[25] and *Igf2r*$^{fl/fl}$ mice[50] by Prof.
294 Bass Hassan (University of Oxford).

295 All strains were bred into an inbred C57BL/6J genetic background for >10 generations. For all crosses,
296 the parent transmitting the floxed allele was also homozygous for the *Rosa26* ^{fl}STOP^{fl}YFP allele. Thus,
297 YFP expression provided an internal control for efficiency of Cre deletion (see Extended Data Fig.
298 1,3,5,8). Genotyping was performed by standard PCR using DNA extracted from ear biopsies (adult
299 mice) or tail DNA (fetuses). PCR was performed using the Red Taq Ready PCR system (Sigma) (see list
300 of primers in Supplementary Table 5), followed by separation of PCR amplicons by agarose gel
301 electrophoresis.

302 **Plasma IGF2 measurements**

303 IGF2 measurements were performed with the Mouse IGF-II DuoSet ELISA kit (R&D Systems – DY792),
304 using an assay adapted for the MesoScale Discovery electrochemiluminescence immunoassay
305 platform (MSD). Briefly, MSD standard-bind microtitre plates were first coated with 30µl capture
306 antibody (Rat Anti-Mouse IGF-II, R&D Systems – 840962) diluted to 7.2 µg/ml in PBS, sealed, and
307 incubated overnight at 4°C. After three washes with MSD wash (0.1% Tween 20 in PBS), the plates

308 were loaded with 20µl ELISA Diluent RD5-38 per well, plus 10µl standard or plasma (diluted 50 fold in
309 RIPA buffer, Sigma – R0278). The plates were then sealed and incubated for two hours at room
310 temperature on a plate shaker. After three washes with MSD wash, the wells were plated with 25µl
311 detection antibody (Biotinylated Goat Anti-Mouse IGF-II, R&D Systems – 840963), diluted to 0.72
312 µg/ml in PBS, sealed, and incubated for one hour at room temperature on a plate shaker. Following
313 three additional washes with MSD wash, the wells were plated with 25µl MesoScale Discovery
314 Streptavidin Sulpho-TAG, diluted 1:1000 in the MSD Diluent 100, sealed and incubated for 30 minutes
315 at room temperature on a plate shaker. After three final washes with MSD wash, the wells were plated
316 with 150µl of MSD Read Buffer T (1x) and the reading was performed on the MSD s600 analyser. Each
317 sample was measured in duplicate and the results were calculated against the standard curve, using
318 the MSD Workbench Software.

319 ***Igf2* mRNA *in situ* hybridization**

320 *In situ* hybridization was performed as described[51], with minor modifications. Briefly, a region of 415bp
321 spanning *Igf2* coding exons 4-6 was PCR amplified using primers: 5'-CACGCTTCAGTTTGTCTGTTCG-3'
322 and 5'-GCTGGACATCTCCGAAGAGG-3' and E14 placental cDNA as template. The PCR amplicon was
323 cloned into a pCR2.1-TOPO plasmid (ThermoFisher Scientific – K450002). Sense (S) and antisense (AS)
324 RNA probes were generated and labelled with Digoxigenin (DIG) by *in vitro* reverse transcription,
325 according to manufacturer's instructions (Roche). E14 fetuses and placentae were collected in ice-cold
326 PBS and fixed overnight in 4% paraformaldehyde in 0.1% diethylpyrocarbonate (DEPC)-PBS at 4°C.
327 Tissues were then dehydrated and embedded in paraffin, using RNase-free conditions. Tissue sections
328 (7µm thick) mounted on polysine slides (VWR) were de-waxed, rehydrated in PBS, post-fixed in 4%
329 paraformaldehyde for 10 minutes, digested with proteinase K (30µg/ml) for 10 min at room
330 temperature, acetylated for 10 minutes (acetic anhydride, 0.25%) and hybridized overnight at 65°C in
331 a humidified chamber with DIG-labeled probes diluted in hybridization buffer. Two 65°C post-
332 hybridization washes (1×SSC, 50% formamide, 0.1% tween-20) followed by two room temperature
333 washes in 1×MABT were followed by 30 minutes RNAse treatment. Sections were blocked for 1 hour
334 in 1×MABT, 2% blocking reagent (Roche), 20% heat-inactivated goat serum and then incubated
335 overnight with anti-DIG antibody (Roche; 1:2,500 dilution) at 4°C. After 4x20 min washes in 1×MABT,
336 slides were rinsed in 1×NTMT and incubated with NBT/BCIP mix in NTMT buffer, according to
337 manufacturer's instructions (Promega). Slides were counterstained with nuclear fast red (Sigma),
338 dehydrated, cleared in xylene and mounted in DPX mounting medium (Sigma). Pictures were taken
339 with an Olympus DP71 bright-field microscope fitted with a camera.

340 **Western blot analysis**

341 Tissues were lysed in ~10µl/mg tissue RIPA buffer (Sigma – R0278), then the lysates were spun at 3,000
342 RPM and 4°C for 15 minutes. The supernatants were transferred into new tubes and protein
343 concentrations were quantified using the Pierce BCA Assay Protein kit (Thermo Scientific – 23225).
344 60µg total protein were mixed with SDS gel loading buffer, then denatured at 70°C for 10 minutes and
345 loaded into 12-well NuPAGE® Novex® 4-12% Bis-Tris precast gels. The pre-stained Novex Sharp protein
346 standard (Invitrogen – LC5800) was used as protein marker. After electrophoresis for 40 minutes at
347 200V and 4°C, the proteins were transferred onto nitrocellulose membranes, using the iBlot® Transfer
348 Stacks (Invitrogen IB 3010-01) and the iBlot® Gel Transfer Device set for 7 minutes at 20V. Blocking
349 was performed for one hour at 4°C in 5% semi-skimmed milk (Marvel) dissolved in TBS-T. The
350 membranes were then incubated overnight at 4°C with the primary antibody dissolved in 0.5% milk in
351 TBS-T (goat anti-human IGF2, 1:1,000, R&D AF292-NA or goat anti-mouse SOD1, 1:50,000, R&D
352 AF3787). After 2x10 minutes washes with milliQ water and 2x10 minutes washes with TBS-T, the blots
353 were incubated for one hour at room temperature with the secondary antibody dissolved in TBS-T

354 containing 3% semi-skimmed milk (rabbit anti-goat IgG-HRP, 1:2,500, Santa Cruz sc-2768). The blots
355 were then washed as above, exposed to substrate (Clarity ECL Western Blotting Substrate, Biorad) for
356 5 minutes and imaged with the Biorad GelDoc system. Stripping of antibodies was carried out using a
357 stripping buffer (ThermoFisher – 21059) for 15 minutes at room temperature. The band intensities
358 were quantified using the ImageLab software (Biorad) and expressed as IGF2/SOD1 ratios.

359 **Placenta stereology**

360 Placenta stereology analyses were performed as described[52] in placentae (n=5–7) collected from three
361 litters at each developmental stage. Briefly, the placentae were weighted, then halved and each half
362 placenta weighted again. A half was fixed in 4% paraformaldehyde in PBS at 4°C overnight, then
363 dehydrated and embedded in paraffin wax. The paraffin blocks were exhaustively sectioned using a
364 microtome at 7µm thickness. Placental sections spaced 140 µm apart were hematoxylin-eosin stained
365 and stereological measurements of placental layers were done using the NewCAST system
366 (Visiopharm, Hoersholm, Denmark), using the point counting method[52].

367 The corresponding placental halves were fixed for 6 hours with 4% glutaraldehyde in 0.1 M PIPES
368 buffer, washed with 0.1 M PIPES buffer, and treated with 1% osmium tetroxide. The samples were
369 then resin-embedded and 1µm thick sections, obtained close to the placental midline, were stained
370 with methylene blue. Analysis of Lz components was done using the NewCAST system (Visiopharm)
371 with meander sampling of ~25% of the Lz area.

372 **Immunostainings**

373 Immunohistochemistry or immunofluorescence conditions are listed in Supplementary Table 6. TUNEL
374 staining was performed using the In Situ Cell Death Detection Kit, TMR red (Sigma – 012156792910),
375 according to manufacturer's protocol. EdU staining was done with the Click-iT® EdU Alexa Fluor 488
376 Imaging Kit (Invitrogen – C10337), according to manufacturer's instructions. For all
377 immunofluorescence stains, DAPI (Sigma – D9542) was used to label the nuclei. For all
378 immunohistochemistry, images were taken with an Olympus DP71 bright-field microscope.
379 Immunofluorescence image acquisition was performed using a LSM510 Meta confocal laser scanning
380 microscope (Carl Zeiss, Jena, Germany) and the ZEN 2009 software. Fluorescence semi-quantification
381 analysis was performed using Volocity 6.3 (Improvision). Counting of TUNEL$^+$ and F4/80$^+$ cells was
382 performed using HALO image analysis software (PerkinElmer).

383 **qRT-PCR analysis**

384 Total RNA was extracted using RNeasy Plus Kits (Qiagen – 74134 and 74034). RNA concentration was
385 measured by NanoDrop (Thermo Scientific) and quality was assessed in agarose gels. RNA extracted
386 from FACS isolated cells was quantified and assessed for quality using the RNA 6000 Pico Kit (Agilent
387 – 5067-1513) and an Agilent 2100 Bioanalyzer. Reverse transcription was performed using the
388 RevertAid RT Reverse Transcription Kit (ThermoFisher – K1622). qRT-PCR was performed with the
389 SYBR Green JumpStart Taq Ready Mix (Sigma – S4438) and custom-made primers (Supplementary
390 Table 7) using an ABI Prism 7900 system (Applied Biosystems). For gene expression normalization, we
391 used four housekeeping genes (*Gapdh*, *Sdha*, *Pmm1*, *Ppia*). Levels of expression were calculated using
392 the $2^{-\Delta\Delta Ct}$ method[53].

393 **Expression microarray analysis**

394 Total RNA was extracted from E19 male placental Lz using RNeasy Midi Kits (Qiagen – 75144) and
395 quantity and quality were verified using RNA 6000 Nano Kit (Agilent – 5067-1511) and an Agilent 2100
396 Bioanalyzer. Only RNA samples with RNA integrity numbers (RIN) >9.0 were used. Array profiling was

397 performed using the Mouse Gene 1.0 ST Array (Affymetrix) and the analysis of the data was performed
398 using GeneSpring GX 12.1 (Agilent, Santa Clara, CA, USA), with two algorithms: RMA (Robust
399 Multiarray Average) and PLIER (Probe Logarithmic Intensity Error). Only genes with $\log_2$ fold change >
400 0.3 predicted by both algorithms were listed as DEGs. Pathway analysis was performed using Ingenuity
401 Pathway Analysis (version 2012).

402 **Flow cytometry analysis of FPEC**

403 Placental labyrinthine layers were micro-dissected in ice-cold PBS. Tissue dissociation into single cells
404 was achieved by digestion at 37°C for 45 minutes with a 0.1% collagenase P solution, aided by
405 mechanical dissociation with needles of decreasing diameter. The cells were then passed through 70-
406 µm cell strainers and washed once in ice-cold PBS + 0.1% BSA. Erythrocytes were lysed using the RBC
407 lysis buffer (BioLegend – 420301). Pelleted cells were then re-suspended in 100µl staining buffer
408 (BioLegend – 420201), counted using the Cedex XS Analyser (Roche) and diluted at 1,000 cells/µl.
409 Blocking of Fc receptors was performed by incubation at 4°C for 20 minutes with an unlabelled anti-
410 CD16/32 (1 µg/million cells; BioLegend – 101320). The cells were then incubated for one hour at 4°C
411 in the dark with a 1:1 mix of anti-mouse CD41 (labelled with Phycoerythrin, PE) (BioLegend – 133906;
412 0.25 µg per million cells) and anti-mouse CD31 (labelled with AF647) (BioLegend – 102516; 0.25 µg
413 per million cells) in 200µl staining buffer. Stained cells were washed twice in 1ml staining buffer, re-
414 suspended in PBS containing a viability marker (7AAD – 7-Aminoactinomycin, Invitrogen – A1310),
415 filtered again through 70-µm cell strainers and incubated on ice for 5 minutes. Flow cytometry analysis
416 was performed with a BD FACSCantoII machine (BD Biosciences) and 100,000 events were recorded
417 for each sample. FSC files were analysed with the FlowJo_V10 software, using single-cell
418 discrimination and gating based on single-stained controls. FPEC were identified as $7AAD^-$
419 $/CD31^+/CD41^-$ cells.

420 **Flow cytometry analysis of FPEC proliferation**

421 Pregnant females received intraperitoneal (i.p.) injections with 50µg of 5-ethynyl-2'-deoxyuridine
422 (EdU)/g body weight, 16 hours prior to tissue collection. Placental Lz dissociation into single cells was
423 performed as above. Cells re-suspended at a concentration of 1000 cells/µl were incubated for 30
424 minutes at 4°C with 1 µl Red LIVE/DEAD Fixable Dead Cell Stain (ThermoFisher – L23102). After one
425 wash in PBS, the cells were pre-incubated for 20 minutes at 4°C in the dark with unlabelled anti-
426 CD16/32 (BioLegend – 101320, 1 µg/million cells), then for 1 hour at 4°C in the dark with a 1:1 mix of
427 anti-mouse CD41 (labelled with BV421, BioLegend – 133911; 0.25 µg per million cells) and anti-mouse
428 CD31 (labelled with AF647) (BioLegend – 102516; 0.25 µg per million cells) in staining buffer. After
429 two washes with staining buffer, the cells were stained using the Click-iT EdU Alexa Fluor 488 Flow
430 Cytometry Assay Kit (ThermoFisher – C10420), according to manufacturer's instructions. Flow
431 cytometry analysis was performed using a BD LSRFortessa cell analyser (BD Biosciences). FSC files were
432 analysed with the FlowJo_V10 software, using single-cell discrimination and gating based on single-
433 stained controls. Proliferating FPEC were identified as viable $EdU^+/CD31^+/CD41^-$ cells.

434 **FPEC isolation by FACS**

435 For sorting, single cell preparation and staining for FPEC markers was performed as above. FACS was
436 done using an Aria-Fusion cell sorter (BD Bioscience), with exclusion of cell duplets and dying cells
437 ($7AAD^+$). Cell fractions (endothelial and non-endothelial cells) were then spun at 3,000 RPM and 4°C
438 for 3 min, the excess of sorting liquid was removed and cell pellets were flash frozen in liquid N_2 and
439 stored at -80°C until used for RNA extraction.

440 **Primary FPEC isolation, culture and tube formation assay**

441 Primary FPEC were isolated as previously described[54] and adapted here to placental Lz (E16). Briefly,
442 placental labyrinthine layers were micro-dissected on ice in RPMI containing 1%
443 penicillin/streptomycin. All samples from one litter were pooled, minced and digested for 90 minutes
444 at 37°C in 2 mg/ml collagenase type I (Sigma) in HBSS containing 2mM CaCl2, 2mM MgSO4, and 20mM
445 HEPES. The digests were filtered through 70µm nylon cell strainers and washed in HBSS. The cell
446 pellets were then resuspended in PBS containing 0.1% BSA and incubated with anti-CD31-coated
447 magnetic beads for one hour at 4°C. Cells coated with beads were cultured in endothelial cell growth
448 medium consisting of low glucose DMEM:F12 with 1% nonessential aminoacids, 2mM sodium
449 pyruvate, buffered with 20mM HEPES and supplemented with 20% FBS and 75µg/ml endothelial
450 mitogens (Sigma – E2759). The cells were incubated at 37°C in 5% O2 and 5% CO2. After four days, the
451 dead cells were washed and new media was added, additionally supplemented with 20µg/ml Heparin
452 (Sigma). Sub-confluent cells (~80%) at passage one (around 10 days in culture) were washed and then
453 cultured in 5% serum replacement media (Sigma – S0638) for ~40 hours. From each litter we used
454 cells at passage one for treatment with 50 ng/ml IGF2 (dissolved in PBS), 1000 ng/ml $IGF2^{Leu27}$
455 (dissolved in 10mM HCl), 500nM PPP (dissolved in DMSO) or 500nM PPP + 50 ng/ml IGF2, or
456 appropriate vehicle control. The cells were harvested with Accutase (Sigma) and counted using the
457 ADAM™ Automated cell counter (NanoEnTek Inc) and 3,000 cells were seeded into 15-well
458 Angiogenesis µ-Slides (Ibidi – 81506) preloaded with 10µl matrigel/well (BD Biosciences – 354234).
459 Photographs were taken at 30 min, 4, 6 and 8 hours using an EVOS FL Cell Imaging system
460 (ThermoFisher Scientific). Each experiment was performed on 5-6 litters for every treatment. For each
461 tube formation assay, we used five wells seeded with primary FPEC exposed to the treatment agent
462 with equivalent numbers of the corresponding vehicle. Quantification of tubular network structures
463 was performed using the Angiogenesis Analyzer software in ImageJ[55].

464 **RNA-sequencing and data analysis**

465 Total RNA was extracted from sorted FPEC by FACS from E16 male placentae using RNeasy Plus Micro
466 Kits (Qiagen – 74034). Quantity and quality were verified using the RNA 6000 Pico Kit (Agilent – 5067-
467 1513) and an Agilent 2100 Bioanalyzer. Only RNA samples with RNA integrity numbers (RIN) >9.0 were
468 used. Total RNA (2 ng) was whole-transcriptome amplified using the Ovation RNA–Seq System V2
469 (NuGEN). To prepare the RNA–seq libraries the amplified cDNA (2µg per sample) was fragmented to
470 200bp using a Bioruptor Sonicator (Diagenode), end repaired and barcoded using the Ovation Rapid
471 DR Library System (NuGEN). The libraries were combined and loaded onto an Illumina HiSeq 2500
472 system for single-end 50bp sequencing at the Genomics Core Facility, Cambridge Institute, CRUK. The
473 reads were aligned onto the mouse GRCm38 genome using TopHat 2.0.11[56]. Gene abundance and
474 differential expression were determined with Cufflinks 2.2.1[57] and expressed in fragments per kilobase
475 per million mapped reads (FPKM). The cut off for expression was set at ≥1 FPKM. Genes with a linear
476 fold expression change greater than 1.5 and a Benjamini–Hochberg false discovery rate (FDR) <5%
477 were considered differentially expressed.

478 Functional analysis was performed using DAVID (Database for Annotation, Visualization and
479 Integrated Discovery; v6.8 http://david.abcc.ncifcrf.gov/). Enriched gene ontology (GO) terms with
480 FDR < 5% were considered significant. These terms were then clustered semantically using REViGO
481 (Reduce and Visualize GO)[58], which removes redundancy, and ordered according to the $\log_{10}$ *P* values.

482 To search for enrichment of TF binding sites at the promoters of DEG, we used EPD (Eukaryotic
483 Promoter Database – https://epd.vital-it.ch/index.php) to retrieve the DNA sequences from 1,000bp
484 upstream to 100bp downstream of the transcriptional start site (TSS). These sequences were then
485 analysed using AME (Analysis of Motif Enrichment v4.12.0 – http://meme-suite.org/tools/ame) by

selecting *Mus musculus* and HOCOMOCO Mouse (v11 FULL) as motif database. Transcriptional network visualization was performed using the Ingenuity Pathway Analysis tool.

Statistical analysis

No statistical analysis was used to predetermine sample size. Randomization was not used in our animal studies. Placental stereology and histological EdU analyses were performed blinded to genotype. All statistical analyses were performed using GraphPad Prism 7. Statistical significance between two groups was determined by Mann-Whitney tests or two-tailed unpaired t-tests and statistical significance between multiple groups was performed using one-way ANOVA plus Tukey's multiple comparisons tests or two-way ANOVA plus Sidak's multiple comparisons tests, as appropriate. The numbers of samples used for each experiment are indicated in figure legends.

Data availability

Expression microarray and RNA-seq data have been deposited in the Gene Expression Omnibus (GEO) (pending accession codes). Other data and materials are available upon request from the corresponding authors.

Acknowledgements

This work was supported by Biotechnology and Biological Sciences Research Council (grant BB/H003312/1 to MC), Medical Research Council (MRC_MC_UU_12012/4 to MC; MRC_MC_UU_12012/5 to the MRC Metabolic Diseases Unit), Centre for Trophoblast Research and the NIHR Cambridge BRC Cell Phenotyping Hub. We thank Nuala Daw, Barbara Villela and Bliss Anderson for technical assistance with the placental stereology analyses, Adrian Wayman and Laura Hunter (West Forvie Phenomics Center) for help with mouse husbandry; Keli Philips and James Warner (Histology Core Facility) for help with preparing tissue samples for histology and F4/80 staining, Gregory Strachan (Imaging Core Facility) for help with TUNEL$^+$ and F4/80$^+$ cells counting using HALO, Marcella Ma (Genomics and Transcriptomics Core) for help with preparing the RNA-Seq libraries and Natalia Savinykh and Esther Perez (NIHR Cambridge BRC Cell Phenotyping Hub) for help with flow cytometry cell sorting.

Contributions

IS and AG performed all the *in vivo* experimental work, with contributions from ASH, SNS, FS, KH, JL-T and AS-P. IS, BYHL and GSHY performed bioinformatics analyses. IS, MR and CMB performed the *in vitro* tube formation assays. KB developed and performed the assay for IGF2 measurements in fetal plasma. IS and MC designed the project and GJB, ALF, AS-P and CMB assisted with the experimental design and data analysis/interpretation. IS, GJB and MC wrote the manuscript, with important contributions from ALF, AS-P and CMB. All other authors discussed the results and edited the manuscript. MC managed and supervised all aspects of the study.

References

1. Fowden, A.L., Ward, J.W., Wooding, F.P., Forhead, A.J. & Constância, M. Programming placental nutrient transport capacity. *J. Physiol.* **572**, 5–15 (2006).
2. Constância, M. *et al.* Adaptation of nutrient supply to fetal demand in the mouse involves interaction between the Igf2 gene and placental transporter systems. *Proc. Natl. Acad. Sci. USA* **102**, 19219–19224 (2005).

527 3. Constância, M. *et al.* Placental-specific IGF-II is a major modulator of placental and fetal growth.
528 *Nature* **417**, 945-948 (2002).
529 4. Angiolini, E. *et al.* Developmental adaptations to increased fetal nutrient demand in mouse
530 genetic models of Igf2-mediated overgrowth. *FASEB J.* **25**, 1737–1745 (2011).
531 5. DeChiara, T.M., Robertson, E.J. & Efstratiadis, A. Parental imprinting of the mouse insulin-like
532 growth factor II gene. *Cell* **64**, 849–859 (1991).
533 6. Baker, J., Liu, J.P., Robertson, E.J. & Efstratiadis, A. Role of insulin-like growth factors in embryonic
534 and postnatal growth. *Cell* **75**, 73–82 (1993).
535 7. Burns, J.L. & Hassan, A.B. Cell survival and proliferation are modified by insulin-like growth factor
536 2 between days 9 and 10 of mouse gestation. *Development* **128**, 3819–3830 (2001).
537 8. Gardner, R.L., Squire,S., Zaina, S., Hills, S. & Graham, C.F. Insulin-like growth factor-2 regulation
538 of conceptus composition: effects of the trophectoderm and inner cell mass genotypes in the
539 mouse. *Biol. Reprod.* **60**, 190–195 (1999).
540 9. Azzi, S., Abi Habib, W. & Netchine, I. Beckwith-Wiedemann and Russell-Silver Syndromes: from
541 new molecular insights to the comprehension of imprinting regulation. *Curr. Opin. Endocrinol.*
542 *Diabetes Obes.* **21**, 30–38 (2014).
543 10. Sferruzzi-Perri, A.N., Sandovici, I., Constancia, M. & Fowden, A.L. Placental phenotype and the
544 insulin-like growth factors: resource allocation to fetal growth. *J. Physiol.* **595**, 5057–5093 (2017).
545 11. Harris, L.K. & Westwood. M. Biology and significance of signalling pathways activated by IGF-II.
546 *Growth Factors* **30**, 1–12 (2012).
547 12. Okamoto, T. *et al.* A simple structure encodes G protein-activating function of the IGF-II/mannose
548 6-phosphate receptor. *Cell* **62**, 709–717 (1990).
549 13. Maeng, Y.S. *et al.* Endothelial progenitor cell homing: prominent role of the IGF2-IGF2R-PLCbeta2
550 axis. *Blood* **113**, 233–243 (2009).
551 14. Wei, Y. *et al.* MetaImprint: an information repository of mammalian imprinted genes.
552 *Development* **141**, 2516–2523 (2014).
553 15. Tallquist, M.D. & Soriano, P. Epiblast-restricted Cre expression in MORE mice: a tool to distinguish
554 embryonic vs. extra-embryonic gene function. *Genesis* **26**, 113–115 (2000).
555 16. Kisanuki, Y.Y. *et al.* Tie2-Cre transgenic mice: a new model for endothelial cell-lineage analysis in
556 vivo. *Dev. Biol.* **230**, 230–242 (2001).
557 17. Augustin, H.G., Koh, G.Y., Thurston, G. & Alitalo, K. Control of vascular morphogenesis and
558 homeostasis through the angiopoietin-Tie system. *Nat. Rev. Mol. Cell Biol.* **10**, 165–177 (2009).
559 18. Austyn, J.M. & Gordon, S. F4/80, a monoclonal antibody directed specifically against the mouse
560 macrophage. *Eur. J. Immunol.* **11**, 805–815 (1981).
561 19. Rawn, S.M. & Cross, J.C. The evolution, regulation, and function of placenta-specific genes. *Annu.*
562 *Rev. Cell. Dev. Biol.* **24**, 159–181 (2008).
563 20. Nagai, A. et al. Cellular expression of the monocarboxylate transporter (MCT) family in the
564 placenta of mice. *Placenta* **31**, 126–133 (2010).
565 21. Hughes, M., Natale, B.V., Simmons, D.G. & Natale, D.R. Ly6e expression is restricted to
566 syncytiotrophoblast cells of the mouse placenta. *Placenta* **34**, 831–835 (2013).
567 22. Rhodes, K.E. et al. The emergence of hematopoietic stem cells is initiated in the placental
568 vasculature in the absence of circulation. *Cell Stem Cell* **2**, 252–263 (2008).
569 23. Wenzel, P.L. & Leone, G. Expression of Cre recombinase in early diploid trophoblast cells of the
570 mouse placenta. *Genesis* **45**, 129–134 (2007).
571 24. Schwenk, F., Baron, U. & Rajewsky, K. A cre-transgenic mouse strain for the ubiquitous deletion
572 of loxP-flanked gene segments including deletion in germ cells. *Nucleic Acids Res.* **23**, 5080–5081
573 (1995).
574 25. Srivastava, M. *et al.* H19 and Igf2 monoallelic expression is regulated in two distinct ways by a
575 shared cis acting regulatory region upstream of H19. *Genes Dev.* **14**, 1186–1195 (2000).

576 26. Lee, N.V. *et al.* ADAMTS1 mediates the release of antiangiogenic polypeptides from TSP1 and 2.
577 *EMBO J.* **25**, 5270–5283 (2006).
578 27. Angiolillo, A.L. *et al.* Human interferon-inducible protein 10 is a potent inhibitor of angiogenesis
579 in vivo. *J. Exp. Med.* **182**, 155–162 (1995).
580 28. Lawler, P.R. & Lawler, J. Molecular basis for the regulation of angiogenesis by thrombospondin-1
581 and -2. *Cold Spring Harb. Perspect. Med.* **2**, a006627 (2012).
582 29. Lankhorst, S., Danser, A.H. & van den Meiracker, A.H. Endothelin-1 and antiangiogenesis. *Am. J.*
583 *Physiol. Regul. Integr. Comp. Physiol.* **310**, R230–R234 (2016).
584 30. Uthaiah, R.C., Praefcke, G.J., Howard, J.C. & Herrmann, C. IIGP1, an interferon-gamma-inducible
585 47-kDa GTPase of the mouse, showing cooperative enzymatic activity and GTP-dependent
586 multimerization. *J. Biol. Chem.* **278**, 29336–29343 (2003).
587 31. Vidal, A. & Koff, A. Cell-cycle inhibitors: three families united by a common cause. *Gene* **247**, 1–
588 15 (2000).
589 32. Fischer, A., Schumacher, N., Maier, M., Sendtner, M. & Gessler, M. The Notch target genes Hey1
590 and Hey2 are required for embryonic vascular development. *Genes Dev.* **18**, 901–911(2004).
591 33. Gregory, J.L. *et al.* Macrophage migration inhibitory factor induces macrophage recruitment via
592 CC chemokine ligand 2. *J. Immunol.* **177**, 8072–8079 (2006).
593 34. Fehniger, T.A. & Caligiuri, M.A. Interleukin 15: biology and relevance to human disease. *Blood* **97**,
594 14–32 (2001).
595 35. Beukers, M.W. *et al.* [Leu27] insulin-like growth factor II is highly selective for the type-II IGF
596 receptor in binding, cross-linking and thymidine incorporation experiments. *Endocrinology* **128**,
597 1201–1203 (1991).
598 36. Girnita, A. *et al.* Cyclolignans as inhibitors of the insulin-like growth factor-1 receptor and
599 malignant cell growth. *Cancer Res.* **64**, 236–242 (2004).
600 37. Bach, L.A. Endothelial cells and the IGF system. *J. Mol. Endocrinol.* **54**, R1–R13 (2015).
601 38. Constância, M., Kelsey, G. & Reik W. Resourceful imprinting. *Nature* **432**, 53–57 (2004).
602 39. Gohlke, B.C., Fahnenstich, H., Dame, C. & Albers, N. Longitudinal data for intrauterine levels of
603 fetal IGF-I and IGF-II. *Horm. Res.* **61**, 200–204 (2004).
604 40. Verhaeghe, J. *et al.* C-peptide, insulin-like growth factors I and II, and insulin-like growth factor
605 binding protein-1 in umbilical cord serum: correlations with birth weight. *Am. J. Obstet. Gynecol.*
606 **169**, 89–97 (1993).
607 41. Tzschoppe, A. et al. Differential effects of low birthweight and intrauterine growth restriction on
608 umbilical cord blood insulin-like growth factor concentrations. *Clin. Endocrinol. (Oxf).* **83**, 739–
609 745 (2015).
610 42. Aoki, A. *et al.* Beckwith-Wiedemann syndrome with placental chorangioma due to H19-
611 differentially methylated region hypermethylation: a case report. *J. Obstet. Gynaecol. Res.* **37**,
612 1872–1876 (2011).
613 43. Armes, J.E. *et al.* The placenta in Beckwith-Wiedemann syndrome: genotype-phenotype
614 associations, excessive extravillous trophoblast and placental mesenchymal dysplasia. *Pathology*
615 **44**, 519–527 (2012).
616 44. Yamazawa, K. *et al.* Molecular and clinical findings and their correlations in Silver-Russell
617 syndrome: implications for a positive role of IGF2 in growth determination and differential
618 imprinting regulation of the IGF2-H19 domain in bodies and placentas. *J. Mol. Med.* **86**, 1171–
619 1181 (2008).
620 45. Mayhew, T.M., Charnock-Jones, D.S. & Kaufmann, P. Aspects of human fetoplacental
621 vasculogenesis and angiogenesis. III. Changes in complicated pregnancies. *Placenta* **25**, 127–139
622 (2004).
623 46. Haley, V.L. *et al.* Igf2 pathway dependency of the Trp53 developmental and tumour phenotypes.
624 *EMBO Mol. Med.* **4**, 705–718 (2012).

47. Dietrich, P., Dragatsis, I., Xuan, S., Zeitlin, S. & Efstratiadis, A. Conditional mutagenesis in mice with heat shock promoter-driven cre transgenes. *Mamm. Genome* **11**, 196–205 (2000).
48. Srinivas, S. *et al.* Cre reporter strains produced by targeted insertion of EYFP and ECFP into the ROSA26 locus. *BMC Dev. Biol.* **1**, 4 (2001).
49. Madisen, L. *et al.* A robust and high-throughput Cre reporting and characterization system for the whole mouse brain. *Nat. Neurosci.* **13**, 133–40 (2010).
50. Wylie, A.A. *et al.* Tissue-specific inactivation of murine M6P/IGF2R. *Am. J. Pathol.* **162**, 321–328 (2003).
51. Simmons, D.G., Rawn, S., Davies, A., Hughes, M. & Cross, J.C. Spatial and temporal expression of the 23 murine Prolactin/Placental Lactogen-related genes is not associated with their position in the locus. *BMC Genomics* **9**, 352 (2008).
52. Coan, P.M., Ferguson-Smith, A.C. & Burton, G.J. Developmental dynamics of the definitive mouse placenta assessed by stereology. *Biol. Reprod.* **70**, 1806–1813 (2004).
53. Livak, K.J. & Schmittgen, T.D. Analysis of relative gene expression data using real-time quantitative PCR and the 2(-Delta Delta C(T)) Method. *Methods* **25**, 402–408 (2001).
54. Branco-Price, C. *et al.* Endothelial cell HIF-1α and HIF-2α differentially regulate metastatic success. *Cancer Cell* **21**, 52–65 (2012).
55. Schneider, C.A., Rasband, W.S. & Eliceiri, K.W. NIH Image to ImageJ: 25 years of image analysis. *Nat. Methods* **9**, 671–675 (2012).
56. Kim, D. *et al.* TopHat2: accurate alignment of transcriptomes in the presence of insertions, deletions and gene fusions. *Genome Biol.* **14**, R36 (2013).
57. Trapnell, C. *et al.* Transcript assembly and quantification by RNA-seq reveals unannotated transcripts and isoform switching during cell differentiation. *Nat. Biotechnol.* **28**, 511–515 (2010).
58. Supek, F., Bošnjak, M., Škunca, N. & Šmuc, T. REVIGO summarizes and visualizes long lists of gene ontology terms. *PLoS One* **6**, e21800 (2011).

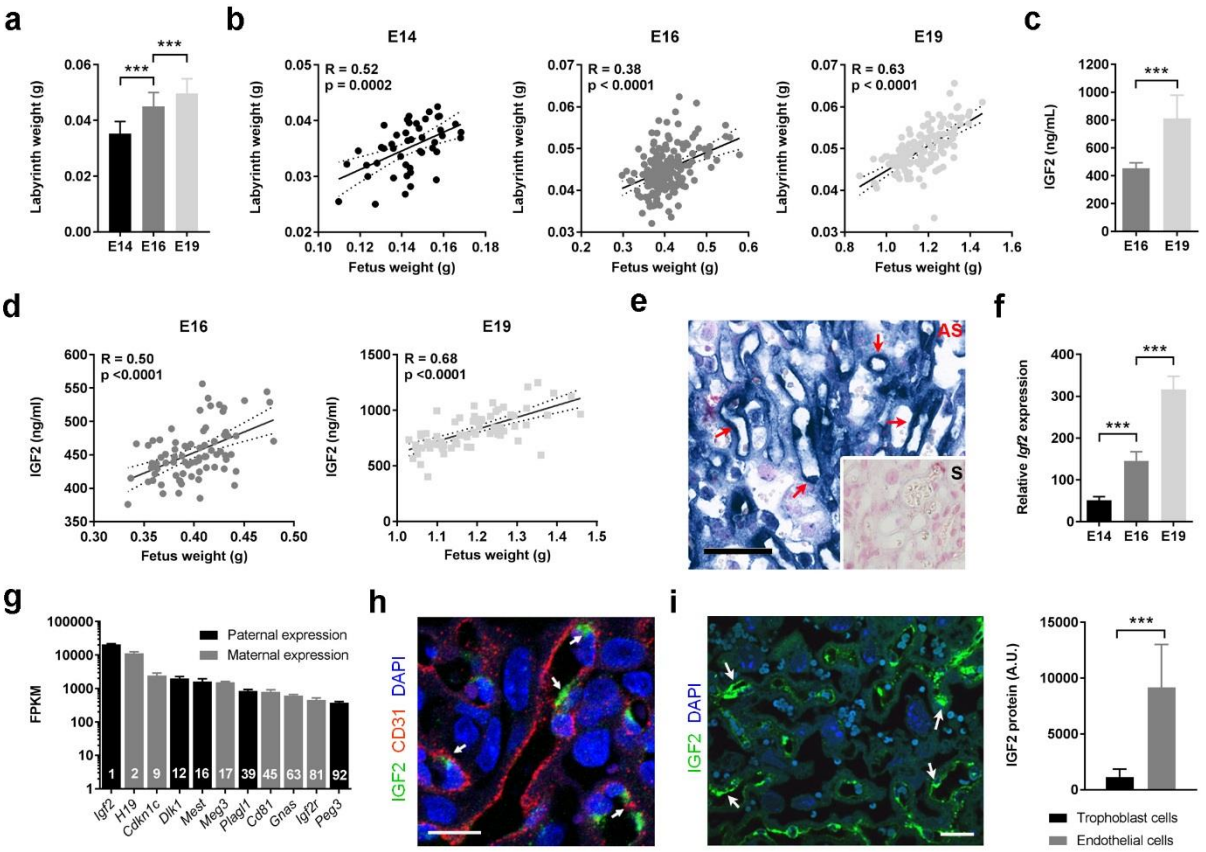

Figure 1: Placental Lz expansion is associated with increasing levels of circulating and endothelial IGF2.

a, Weights of micro-dissected Lz. **b,** Linear correlation analyses between fetal and placental Lz weights (n=46–189 placentae from n>10 litters per group in **a**, **b**). **c,** Levels of IGF2 (ng/mL) in plasma of wild-type fetuses. **d,** Linear correlation analyses between fetal weights and circulating IGF2 (n=70–79 per group in **c**, **d**). **e,** *Igf2* mRNA *in situ* hybridization (blue) in E14 wild-type placental Lz (red arrows– FPEC; AS – antisense probe; inset with sense probe – S; scale bar is 50µm). **f,** Relative *Igf2* mRNA expression levels measured by qRT-PCR in FPEC from wild-type placental Lz (n=6–7 per group). **g,** Imprinted genes that rank within top 100 expressed genes in E16 wild-type FPEC (FPKM – Fragments Per Kilobase Million; n=4). **h,** Double immunostaining for IGF2 and CD31 in E19 wild-type placenta, demonstrating expression in FPEC. Endothelial cells are very thin and hard to detect except where the cytoplasm is more voluminous around the nucleus, with intense IGF2 stain (white arrows). Transmembrane glycoprotein CD31 immunostaining is in the membrane and largely marks endothelial intercellular junctions (scale bar is 20µm)**. i,** Semi-quantitative measurement of IGF2 protein in FPEC versus trophoblast cells (E19 wild-type placental Lz, n=60 cells per group from two placentae). White arrows – endothelial cells; scale bar is 50µm. Data (**a**, **c**, **f**, **g**, **i**) is presented as averages ± standard deviation (SD); *** *P*<0.001 calculated by one-way ANOVA plus Tukey's multiple comparisons test (**a, f**) or by unpaired *t*-test with Welch's correction (**c**, **i**).

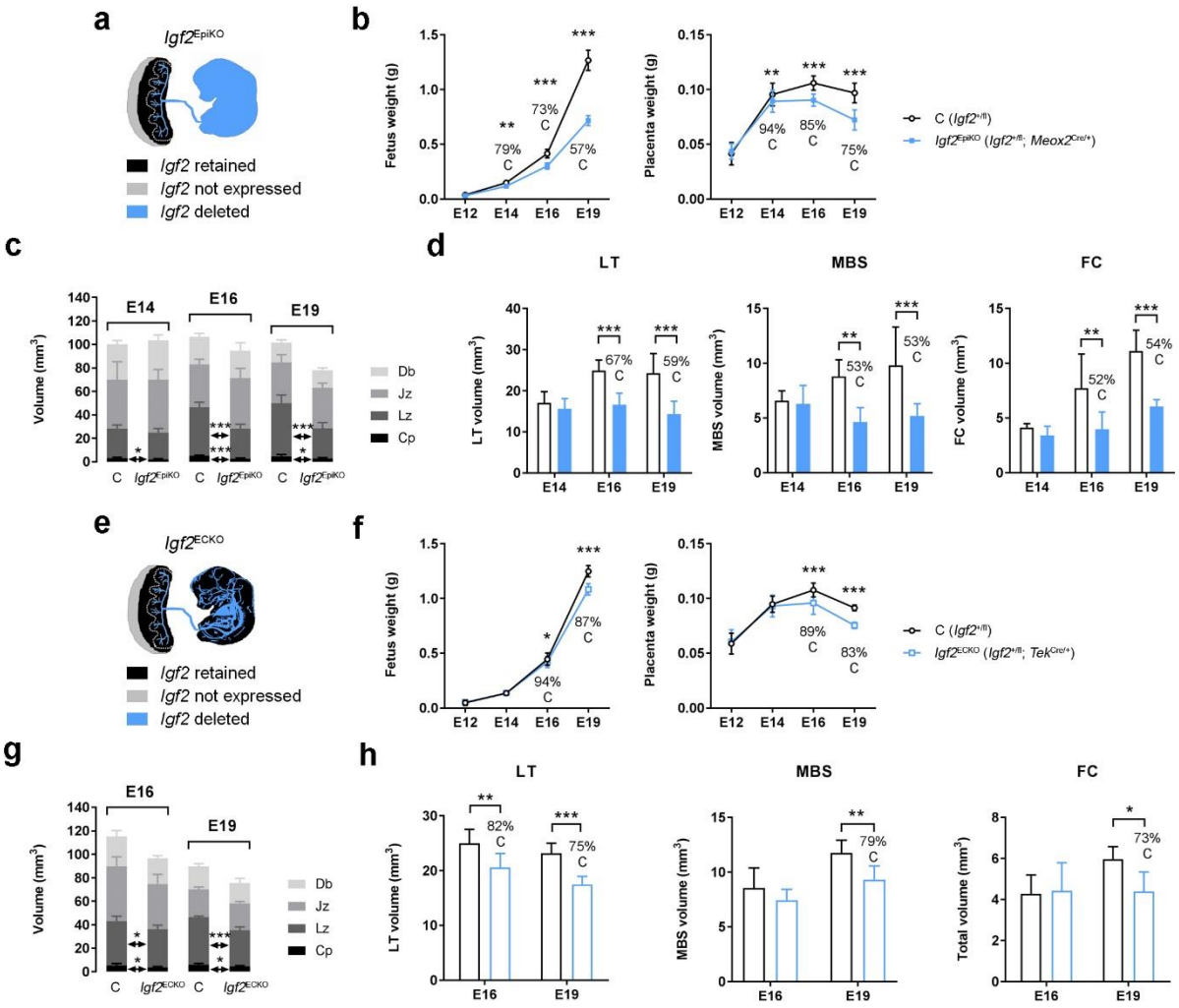

Figure 2: Deletion of *Igf2* in the epiblast or endothelium impairs placental Lz expansion.

a, Schematic of *Igf2* expression in conceptuses with conditional deletion driven by *Meox2*^{Cre}. **b,** Fetal and placental growth kinetics (E12: n=10 litters; E14: n=22 litters; E16: n=36 litters; E19: n=34 litters). **c,** Absolute volumes of the placental layers (Db – decidua basalis, Jz – junctional zone, Lz – labyrinthine zone, Cp – chorionic plate), measured by stereology. **d,** Absolute volumes (in mm^3) of placental Lz components, measured by stereology (LT – labyrinthine trophoblast, MBS – maternal blood spaces, FC – fetal capillaries) (n=6 per group). **e,** Schematic of *Igf2* expression in conceptuses with conditional deletion driven by *Tek*^{Cre}. **f,** Fetal and placental growth kinetics (E12: n=4 litters; E14: n=8 litters; E16: n=13 litters; E19: n=7 litters). **g,** Absolute volumes of the placental layers measured by stereology (n=5–7 per group). **h,** Absolute volumes (in mm^3) of placental Lz components, measured by stereology. For all graphs data is shown as averages; error bars represent SD; * P<0.05; ** P<0.01; *** P<0.001 calculated by two-way ANOVA plus Sidak's multiple comparisons tests (**b**, **d**, **f**, **h**) or unpaired t tests (**d**, **g**).

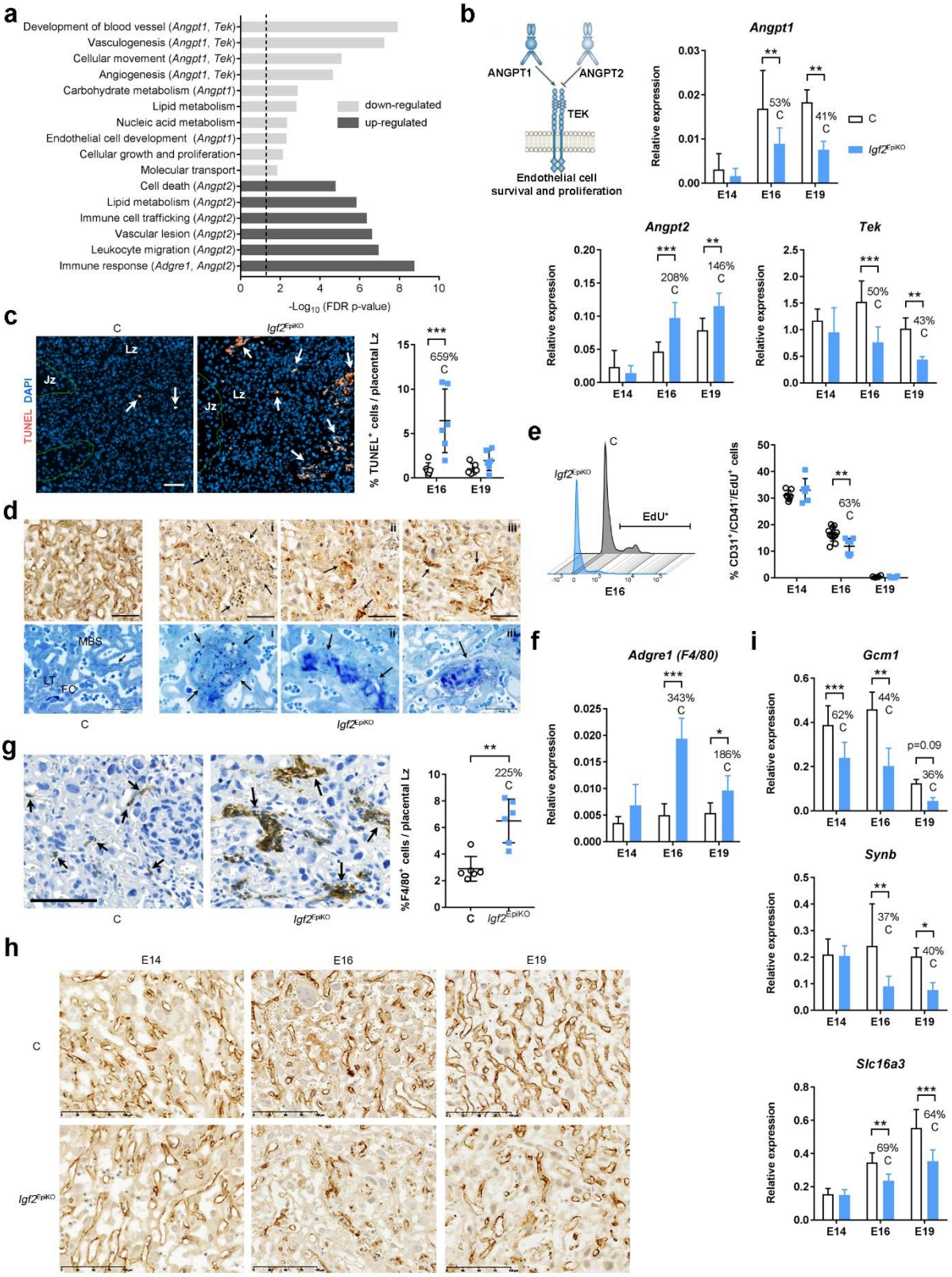

Figure 3: Lack of fetus-derived IGF2 reduces the expansion of feto-placental microvasculature in late gestation.

701 **a,** Functions enriched in DEGs at E19. **b,** qRT-PCR analysis of angiopoietin-Tie2/TEK signalling
702 components in placental Lz (n=6–8 per group). **c,** TUNEL staining in E16 placental Lz (arrows point to
703 apoptotic cells) and data quantification (n=6 samples per group); scale bar is 50µm. **d,** Top row: CD31
704 staining in control (C) and *Igf2*^{EpiKO} mutant E16 placental Lz illustrating abnormally large FCs lacking
705 endothelial cells (i) or obstructed capillaries surrounded by fragmented and disorganized FPEC (ii, iii).
706 Scale bars are 50µm. Bottom row: methylene blue-stained E16 placental Lz resin sections (arrows
707 indicate a FPEC in C and thrombotic FC in mutants: i-iii). Scale bars are 30µm. **e,** FPEC proliferation
708 measured by flow cytometry (left – representative histograms at E16; right – data quantification; n=4–
709 11 per group). **f,** qRT-PCR analysis of *Adgre1* in placental Lz. **g,** Representative F4/80 immunostainings
710 in E16 placental Lz (arrows indicate macrophages). Scale bar is 100µm. Right: percentage of
711 macrophages/placental Lz at E16 (n=6–8 samples per group). **h,** Representative CD31 immunostaining
712 in placental Lz (scale bar is 100µm). **i,** Top: qRT-PCR analysis for SynT-II (syncytiotrophoblast layer II)
713 marker genes. For all graphs data is presented as averages or individual values; error bars are SD; *
714 $P<0.05$, ** $P<0.01$, *** $P<0.001$ by two-way ANOVA plus Sidak's multiple comparisons tests (**b**, **c**, **e**, **f**,
715 **i**) or Mann-Whitney tests (**g**).

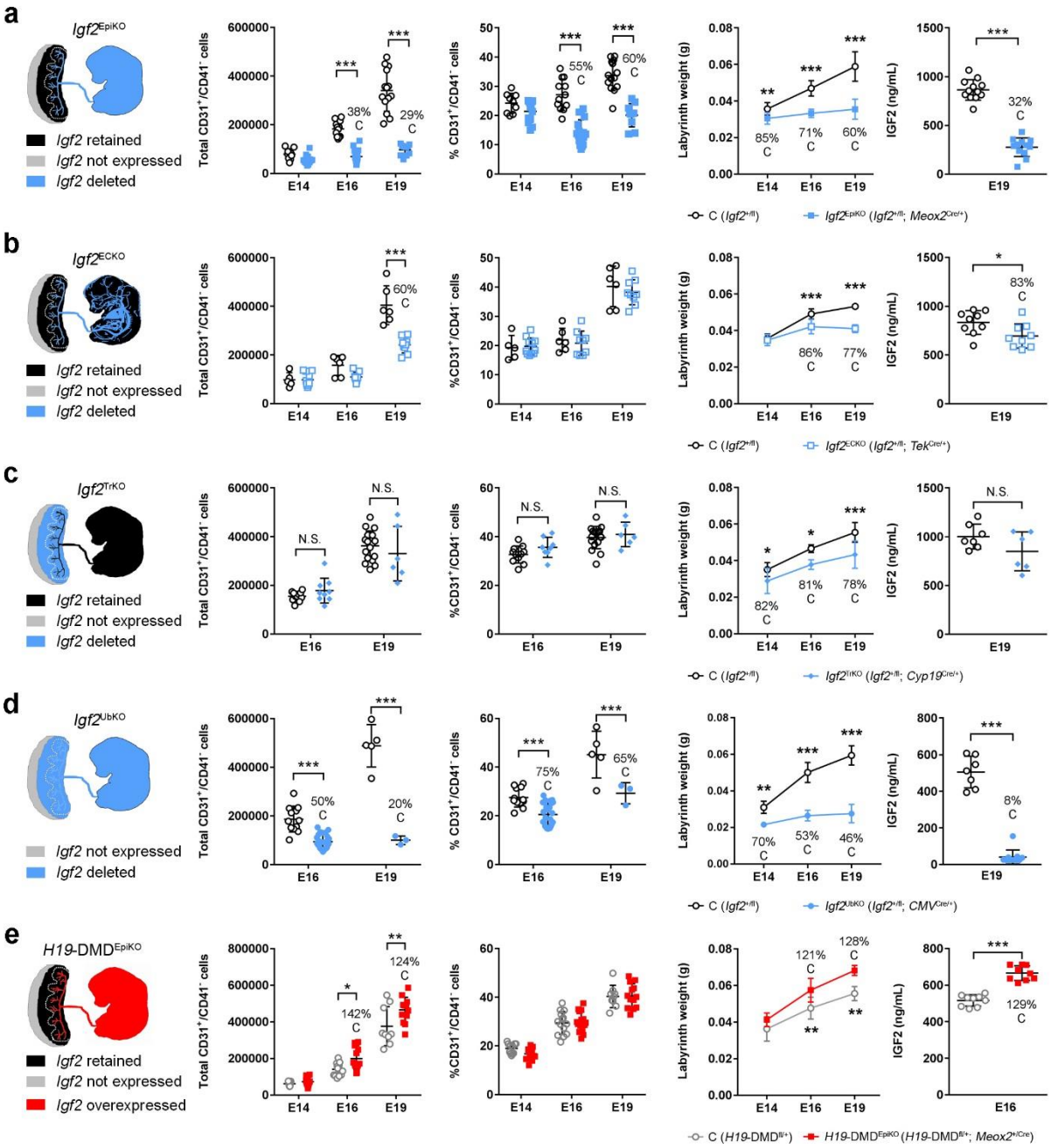

Figure 4: Genetic models of mismatched supply and demand reveal circulating IGF2 as a major endocrine regulator of FPEC and placental Lz expansion.

Column 1: schematic diagram of the genetic models: *Igf2*^{EpiKO} (**a**), *Igf2*^{ECKO} (**b**), *Igf2*^{TrKO} (**c**), *Igf2*^{UbKO} (**d**) *H19*-DMD^{EpiKO} (**e**). Columns 2 and 3: total numbers (column 2) and proportion of FPEC/placental Lz (column 3), measured by flow cytometry (n conceptuses per group: *Igf2*^{EpiKO}: n=9–18; *Igf2*^{ECKO}: n=5–11; *Igf2*^{TrKO}: n=6–17; *Igf2*^{UbKO}: n=3–26; *H19*-DMD^{EpiKO}: n=9–15). Column 4: placental Lz growth kinetics (*Igf2*^{EpiKO}: n=9–20 litters; *Igf2*^{ECKO}: n=3–9 litters; *Igf2*^{TrKO}: n=4–9 litters; *Igf2*^{UbKO}: n=3–8 litters; *H19*-DMD^{EpiKO}: n=3–4 litters). Column 5: IGF2 levels (ng/mL) in plasma (n per group: *Igf2*^{EpiKO}: n=12; *Igf2*^{ECKO}: n=9; *Igf2*^{TrKO}: n=6–7; *Igf2*^{UbKO}: n=7–11; *H19*-DMD^{EpiKO}: n=9). Data is shown as averages or individual values and error bars are SD. N.S. – not significant; * $P<0.05$; ** $P<0.01$; *** $P<0.001$ calculated by two-way ANOVA plus Sidak's multiple comparisons tests (second, third and fourth columns) or Mann Whitney tests (fifth column).

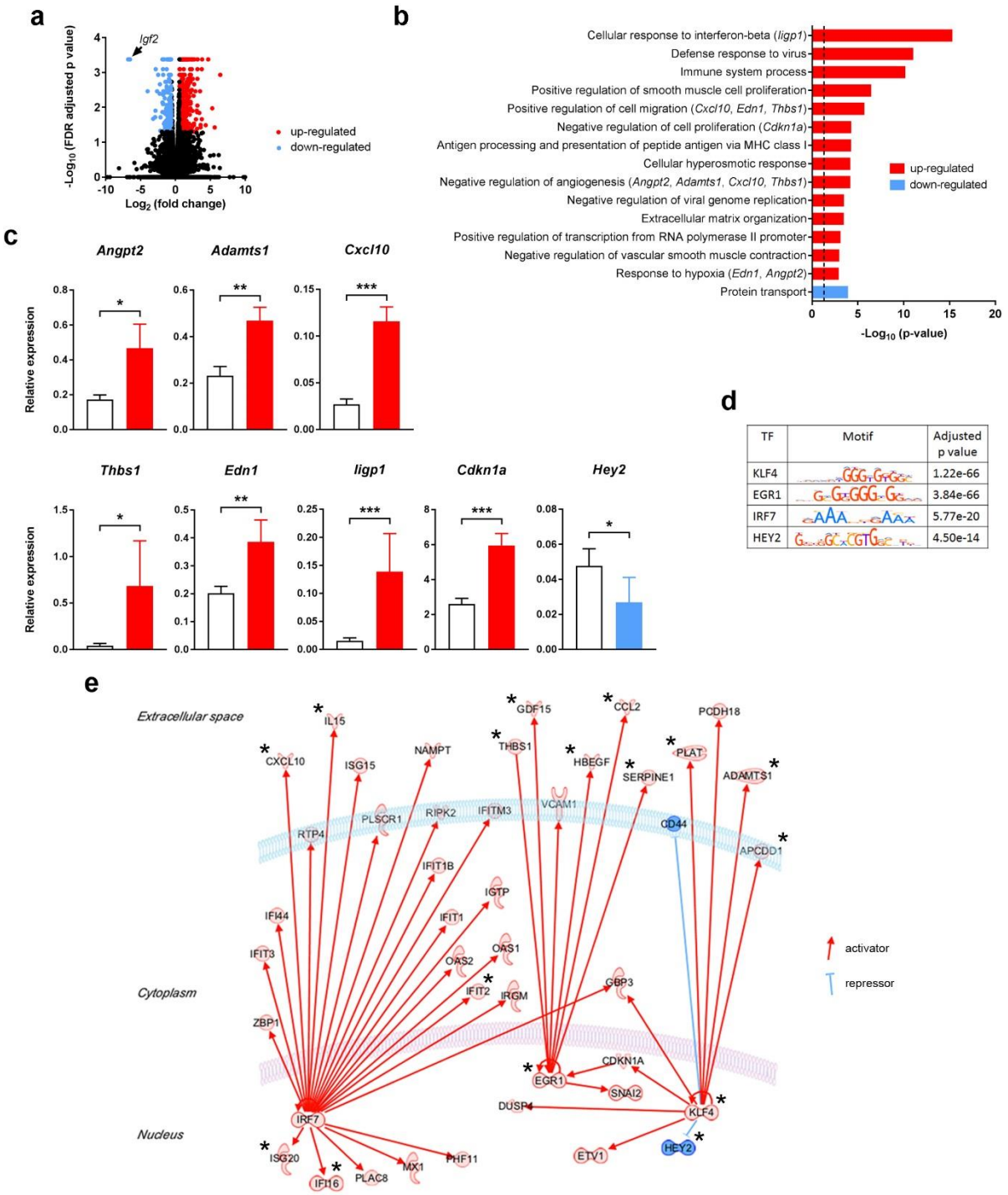

Figure 5: IGF2 signalling regulates angiogenic properties of endothelial cells.

a, Volcano plot representation of DEGs identified by RNA-seq in E16 FPEC (*Igf2*^{EpiKO} versus controls). Significant up-regulated (red) and down-regulated (blue) DEGs (FDR<0.05). **b,** Top scoring biological processes enriched in DEGs. Biologically validated DEGS are listed in parentheses. The dotted line corresponds to FDR-corrected *P* value of 0.05. **c**, Biological validation. Data is shown as averages (n=11-12 samples per group); error bars are SEM; * *P*<0.05, ** *P*<0.01, *** *P*<0.001 calculated by Mann-Whitney tests. **d,** Transcription factors (TFs) identified by Analysis of Motif Enrichment (AME) **e**, IPA regulatory network built with the four TFs identified using AME analysis. Proteins labelled with * are

known regulators of angiogenesis (angiostatic or pro-angiogenic factors) and key references are listed in Supplementary Table 4.

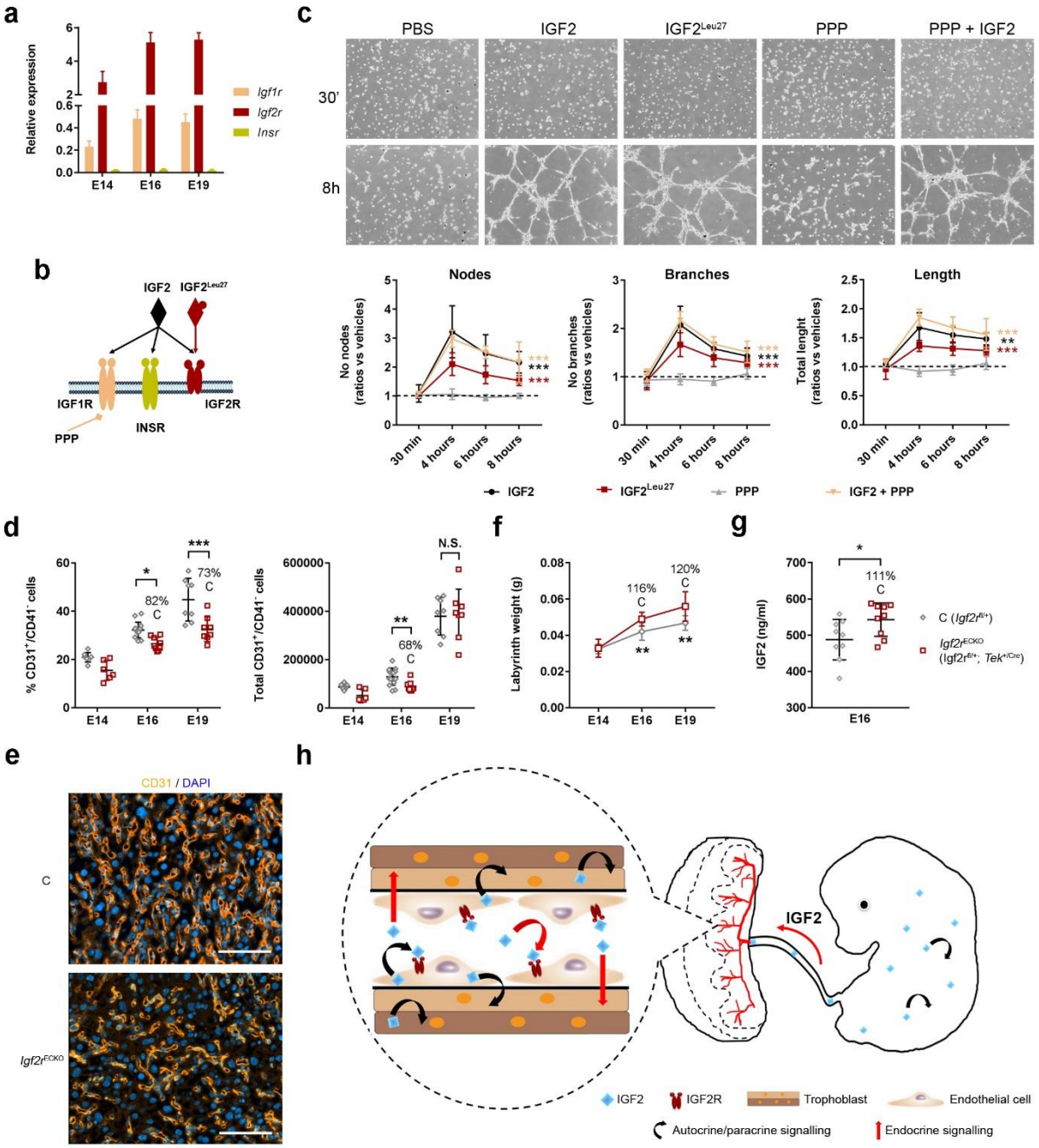

Figure 6: IGF2 acts on feto-placental endothelial cells via IGF2R both *in vitro* and *in vivo*.

a, qRT-PCR analysis for *Igf1r*, *Igf2r* and *Insr* in primary FPEC (n=6–7 per group). **b,** Schematic representation of IGF2 and IGF receptors. IGF2^{Leu27} analogue acts specifically on IGF2R and picropodophyllin (PPP) inhibits phosphorylation of IGF1R. **c,** Representative images of capillary-like tube formation assay in primary FPEC seeded on matrigel and exposed to exogenous IGF2, IGF2^{Leu27},

750 PPP or PPP+IGF2 (equal seeding of cell numbers at 30' and tube formation at 8h), and quantification
751 of number of nodes, branches and total length (n=5–6 independent experiments). **d,** Proportion and
752 total numbers of FPEC/placental Lz measured by flow cytometry (n=6–14 per group). **e,**
753 Representative CD31 immunofluorescence staining in E16 placental Lz (scale bar is 100µm). **f,**
754 Placental Lz growth kinetics: *Igf2r*^{ECKO} (n=8–16 conceptuses per group). **g,** IGF2 levels (ng/mL) in plasma
755 at E16 (n=9 per group). **h,** Model summarizing the proposed actions of fetus-, endothelial- and
756 trophoblast-derived IGF2. For all graphs, data is presented as averages or individual values and error
757 bars represent SD (**a**, **d**, **e**, **g**) or SEM (**c**). N.S. – not significant; * $P<0.05$; ** $P<0.01$; *** $P<0.001$
758 calculated by two-way ANOVA tests (**c**); two-way ANOVA plus Sidak's multiple comparisons tests (**d**, **f**)
759 or Mann Whitney tests (**g**).

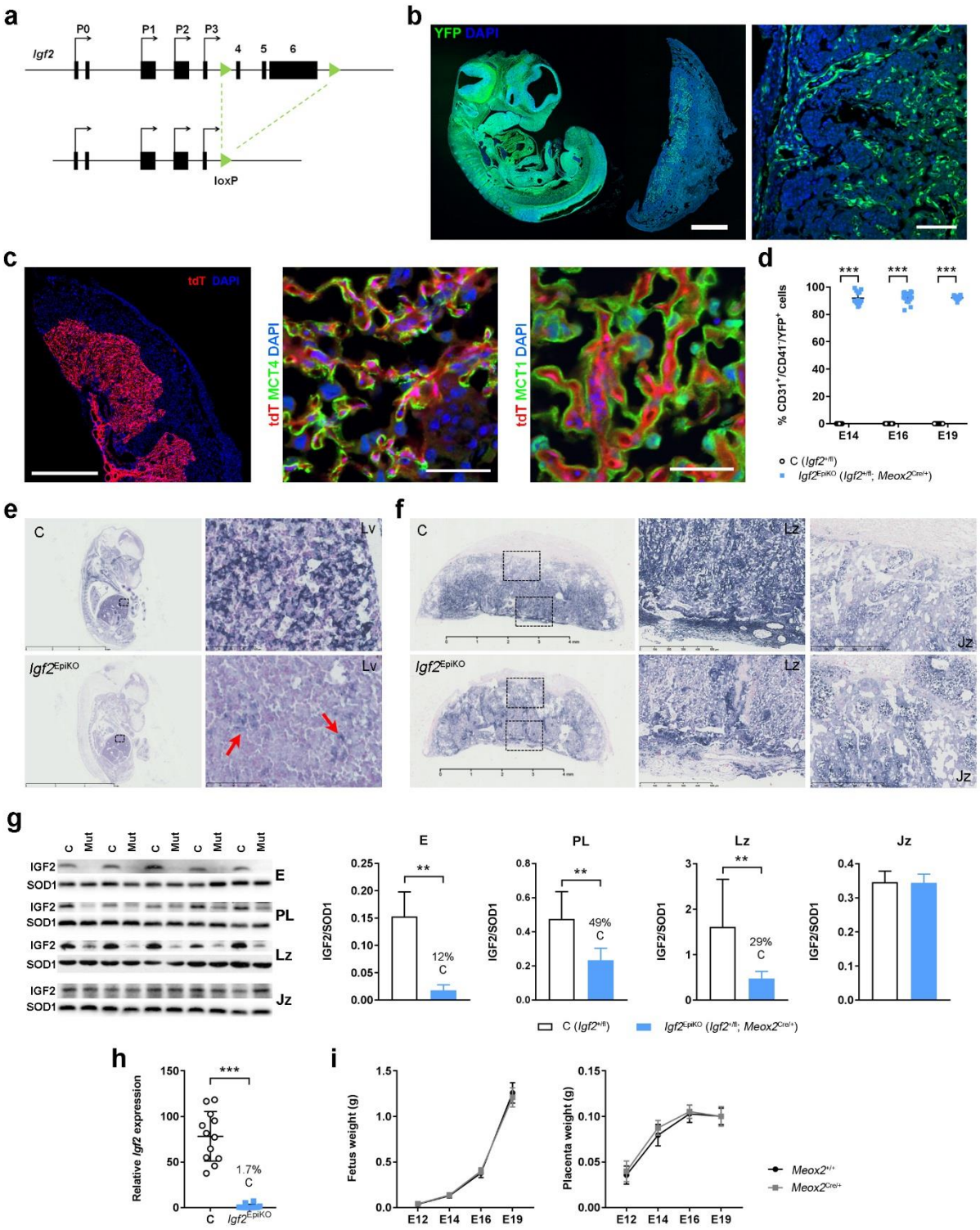

Extended Data Figure 1: Specificity and efficiency of *Igf2* deletion in fetal tissues and feto-placental endothelial cells by *Meox2*^{Cre}.

a, Schematic representation of the floxed *Igf2* allele. P0-P3 are alternative promoters. Protein-coding exons (4–5), flanked by loxP sites (green triangles), are excised upon Cre-loxP mediated recombination. **b,** Immunostaining for YFP (green) in a representative fetus and placenta at E12 of gestation, double transgenic for *Meox2*^{Cre} and *Rosa26* ^{fl}STOP^{fl}YFP[10] reporter. YFP expression is observed throughout the fetus and in the placenta is localized to the labyrinthine zone and chorionic

768 plate (right panel). Blue – DAPI stain for nuclei; scale bars are 1 mm (left) and 100 µm (right). **c,**
769 Representative confocal microscopy of a placental frozen section at E16 of gestation, double
770 transgenic for *Meox2*^{Cre} and Ai9(RCL-tdT) reporter. The *Meox2*^{Cre} is not expressed in the
771 syncytiotrophoblast layers, as demonstrated by the lack of immunostaining overlap between the
772 tomato protein (red) and MCT4 (a marker of the syncytiotrophoblast layer II, facing the feto-placental
773 capillaries) or MCT1 (marker of the syncytiotrophoblast layer I, facing the maternal blood spaces).
774 Scale bars are 1 mm (left panel) and 50 µm (middle and right panels). **d,** Flow cytometry analysis shows
775 that the majority (>80%) of *Igf2*^{EpiKO} mutant FPEC (CD31^{+}/CD41^{-} cells) express YFP (activated by
776 *Meox2*^{Cre} mediated deletion of the *Rosa26* ^{fl}STOP^{fl}YFP STOP cassette), thus demonstrating good
777 efficiency of *Meox2*-Cre in these cells (n=9–18 per genotype). **e,** *Igf2* mRNA in situ hybridization (ISH)
778 in E14 control and mutant fetuses. Dark blue indicates *Igf2* mRNA, with nuclei marked in red. Insets
779 illustrate efficient *Igf2* deletion in the liver (Lv); arrows – small pockets of cells with incomplete *Igf2*
780 deletion (mosaic activity of *Meox2*^{Cre}). Scale bars are 6 mm (left) and 100 µm (right). **f,** *Igf2* mRNA ISH
781 in E14 control and mutant placentae. Insets show reduced *Igf2* mRNA signal in the placental
782 labyrinthine zone (Lz) of mutants, due to its deletion from FPEC, while *Igf2* expression is unchanged in
783 the junctional zone (Jz). Scale bars are 4 mm (left) and 500 µm (right). **g,** Western blot analysis of pro-
784 IGF2 (18kDa) in cell lysates from whole fetuses (F), whole placenta (PL) micro-dissected placental
785 labyrinthine (Lz) and junctional zones (Jz) at E14, and corresponding data quantification shown as
786 graphs (n=5 per genotype). SOD1 (19 kDa) was used as loading control. **h,** Efficiency of *Igf2* deletion
787 evaluated by qRT-PCR in fluorescence-activated sorted FPEC (n=12 per genotype). **i,** Fetal and
788 placental growth kinetics are not altered in *Meox2*$^{Cre/+}$ carriers (maternal inheritance) (n=8–30
789 conceptuses per genotype at each developmental stage). For all graphs, data is shown as individual
790 values or averages ± SD; ** $P < 0.01$, *** $P < 0.001$ calculated by two-way ANOVA plus Sidak's multiple
791 comparisons tests (**d**) or Mann Whitney tests (**g**, **h**).

792

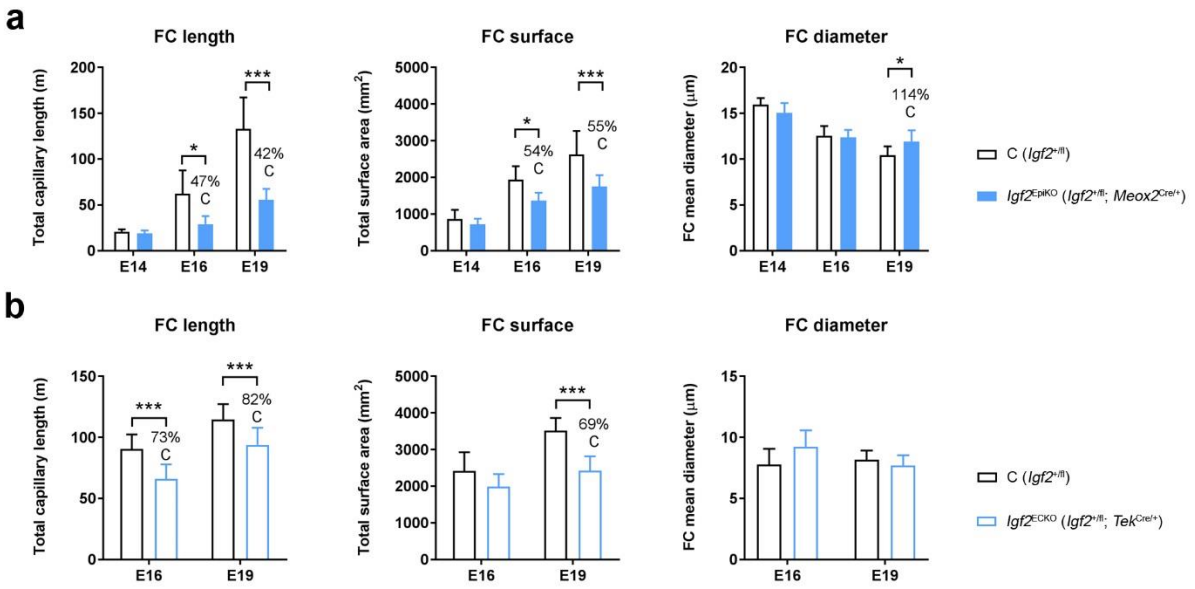

793

794

795 **Extended Data Figure 2: Impact of *Igf2*^{EpiKO} and *Igf2*^{ECKO} deletions on feto-placental capillary**
796 **expansion during gestation.**

a, Parameters of feto-placental capillaries (FC) measured by stereology in *Igf2*^{EpiKO} mutant (*Igf2*$^{+/fl}$; *Meox2*$^{Cre/+}$) versus control (C – *Igf2* $^{+/fl}$) placentae (n=6 per genotype at each developmental stage). **b,** Parameters of feto-placental capillaries (FC) measured by stereology in *Igf2*^{ECKO} mutant (*Igf2*$^{+/fl}$; *Tek*$^{Cre/+}$) versus control (C – *Igf2* $^{+/fl}$) placentae (n=5–7 per genotype at each developmental stage). For all graphs, data is shown as averages ± SD; * $P < 0.05$, *** $P < 0.001$ calculated by two-way ANOVA plus Sidak's multiple comparisons tests.

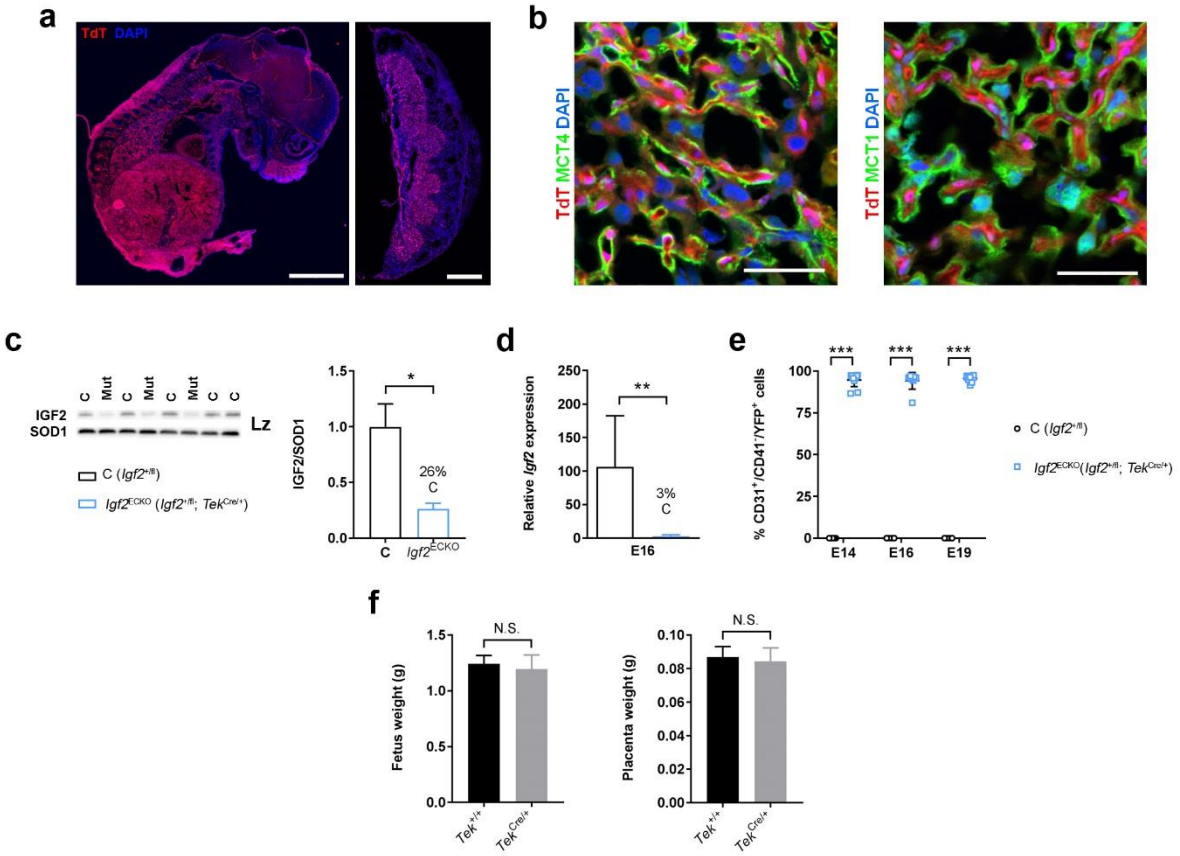

Extended Data Figure 3: Specificity and efficiency of *Igf2* deletion in the endothelium by *Tek*^{Cre}.

a, Representative confocal microscopy of frozen sections from a fetus and corresponding placenta, double transgenic for *Tek*^{Cre} and Ai9(RCL-tdT) reporter at E16 of gestation. Scale bars are 2 mm (fetus) and 1 mm (placenta). **b,** The *Tek*^{Cre} is not expressed in the syncytiotrophoblast layers, as demonstrated by the lack of immunostaining overlap between the tomato protein (red) and MCT4 (Syn-TII layer) or MCT1 (Syn-TI layer). Scale bars are 50 µm. **c,** Western blot analysis of pro-IGF2 (18 kDa) in cell lysates from placental Lz micro-dissected at E16 and corresponding data quantification (n=3 per genotype). SOD1 (19 kDa) was used as internal control for loading. **d,** Efficiency of *Igf2* deletion evaluated by qRT-PCR in fluorescence-activated sorted FPEC (n=5–7 per genotype). **e,** Flow cytometry analysis shows that the majority (>80%) of *Igf2*^{ECKO} mutant FPEC express YFP, thus demonstrating good efficiency of *Tek*^{Cre} in these cells (n=5–11 per genotype). **f,** Fetal and placental growth kinetics are not altered in *Tek*$^{Cre/+}$ carriers (maternal inheritance) at E19 (n=13–15 conceptuses per genotype from 4 independent litters).

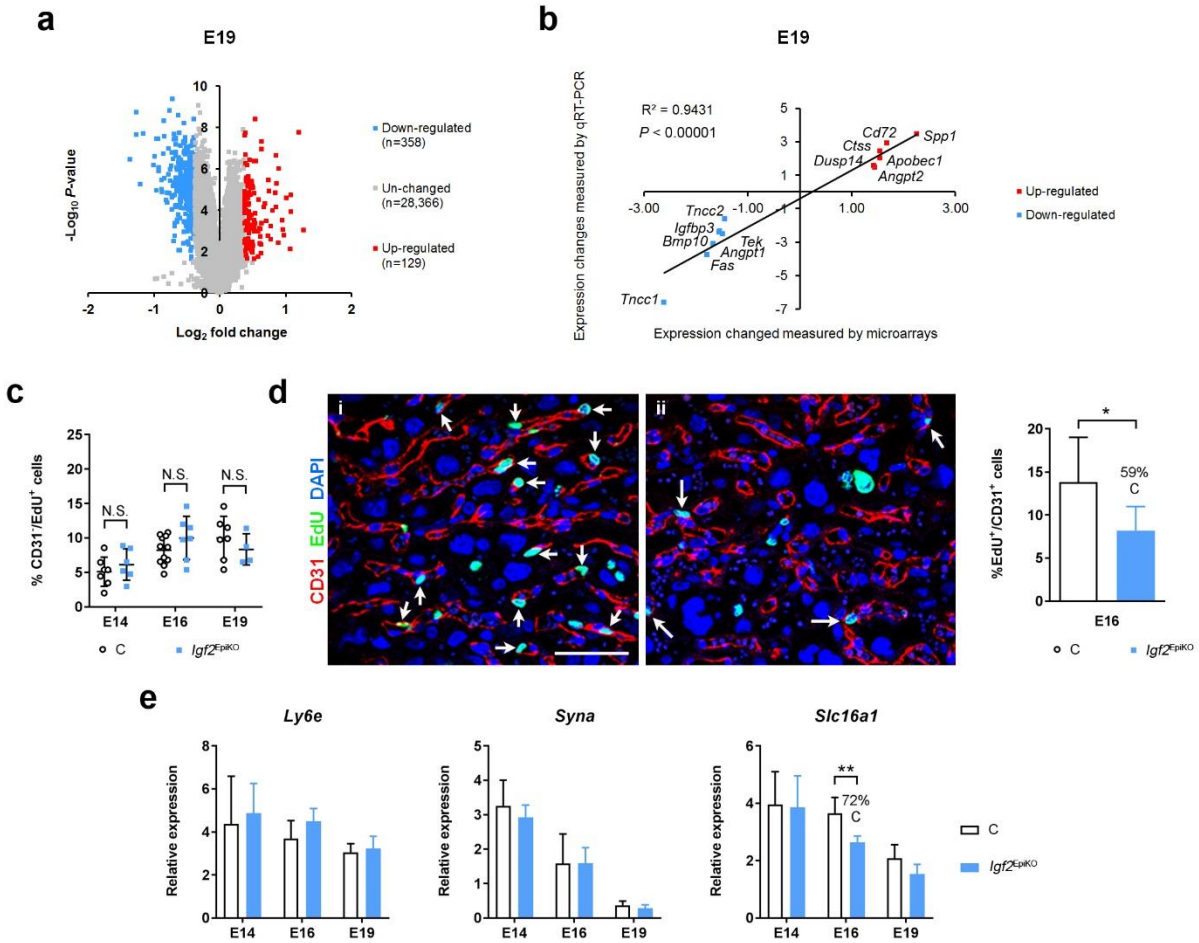

Extended Data Figure 4: Fetus-derived *Igf2* deletion (*Igf2*^{EpiKO}) alters gene expression in placental Lz and FPEC proliferation.

a, Volcano plot depicting differentially expressed genes (DEG) identified in E19 placental Lz by expression microarray analysis (n=6 samples per genotype, all from male conceptuses). **b,** Biological validation using qRT-PCR for 13 DEGs (n=6–7 samples per genotype), normalized against three housekeeping genes (*Sdha*, *Gapdh* and *Pmm1*). **c,** The reduction in proliferation seen in FEPC (Fig. 3e) is not observed in non-endothelial cells from placental Lz measured by flow cytometry analysis after EdU injections (16 hours exposure; n=4–11 per group). **d,** Representative confocal microscopy image of FPEC proliferation in control (panel i) versus mutant (panel ii) E16 placentae by immunofluorescent staining for CD31 combined with Click-iT EdU imaging. Arrows point towards FPEC nuclei that incorporated EdU *in vivo* during the 16 hours exposure to the thymidine analogue. Scale bar is 50 µm. The accompanying graph shows data quantification based on counting between 250 to 600 FPEC per sample (n=6 placentae/genotype). **e,** qRT-PCR analysis of genes expressed in Syn-TI in micro-dissected placental Lz in mutants versus controls (n=6–8 samples per group for each developmental time point). For all graphs, data is presented as averages or individual values ± SD; N.S. – non-significant, * $P < 0.05$, ** $P < 0.01$, by two-way ANOVA plus Sidak's multiple comparisons tests (**c**, **e**) or Mann Whitney test (**d**).

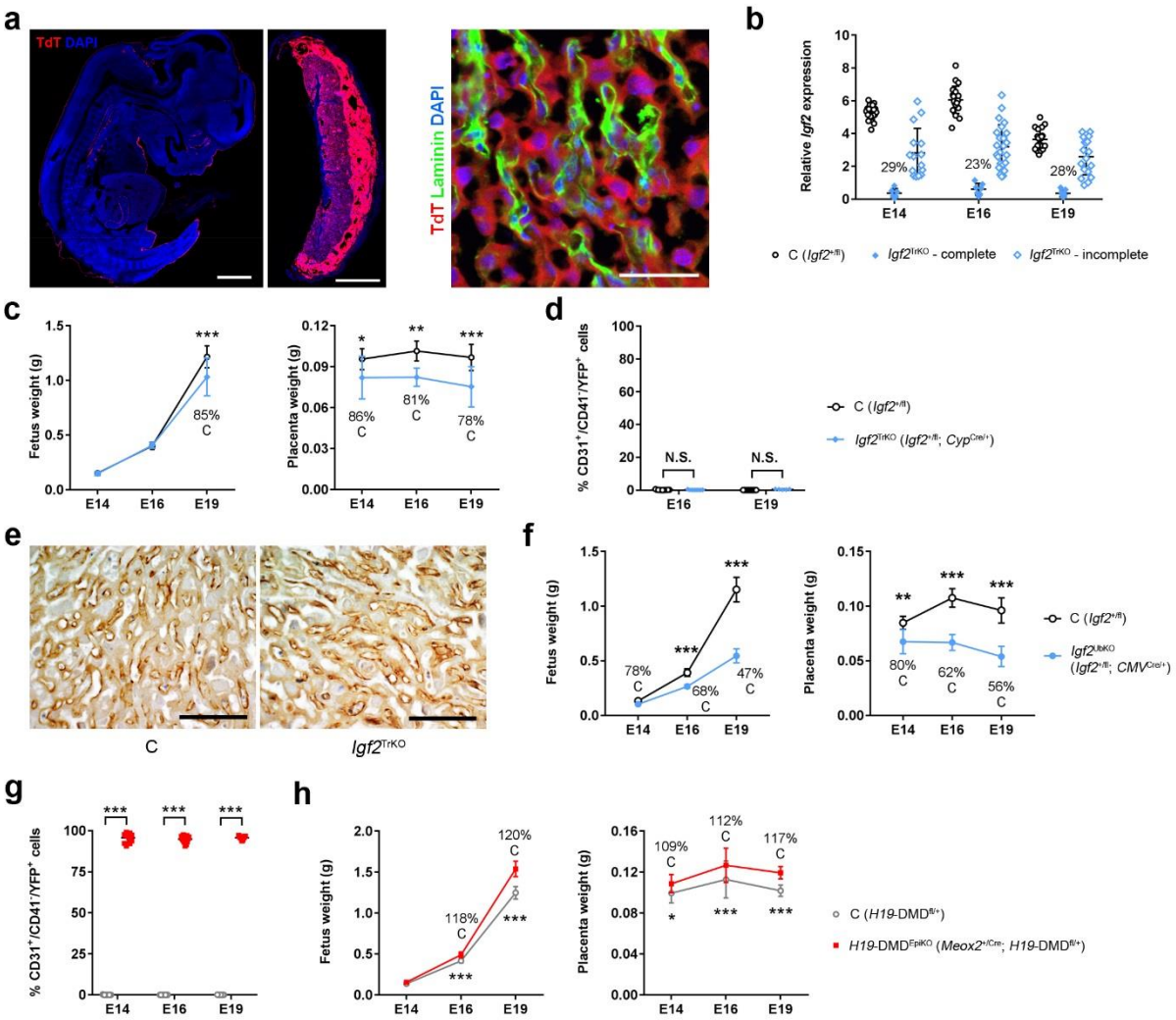

Extended Data Figure 5: Specificity and efficiency of *Igf2*^{TrKO}, *Igf2*^{UbKO} and *H19*-DMD^{EpiKO} deletions.

a, Representative confocal microscopy on frozen sections from a double transgenic Ai9(RCL-tdT), *Cyp19*^{Cre} fetus and corresponding placenta, at E16, demonstrating high Cre activity (red) in placenta and weak activity in embryonic skin and eye lenses. Right panel: *Cyp19*^{Cre} is only active in the trophoblast cells in placental Lz, as demonstrated by lack of overlapping between the tomato protein (red) and laminin (green) expressed in FPEC. Scale bars are 1 mm (left and middle panel) or 50 µm (right panel). **b,** Efficiency of *Igf2* deletion by *Cyp19*^{Cre} in *Igf2*^{TrKO} mutants (*Igf2*$^{+/fl}$; *Cyp19*$^{Cre/+}$) versus controls (*Igf2*$^{+/fl}$) evaluated using qRT-PCR in micro-dissected placental Jz layer (n=20–31 samples per genotype). Only 23-29% of all *Igf2*^{TrKO} mutants have high levels of deletion (>80%). **c,** Placenta growth restriction precedes fetal growth restriction in *Igf2*^{TrKO} mutants (n=4–9 litters at each developmental stage; only mutants with >80% deletion were included in this analysis). **d,** Flow cytometry analysis showing that *Cyp19*^{Cre} is not expressed in FPEC (note lack of YFP expression in *Igf2*^{TrKO} mutants) (n=6–21 per genotype). **e,** Representative CD31 immunostainings in E16 control and *Igf2*^{TrKO} placental Lz (scale bars are 100µm) showing no impact of the deletion on FPEC numbers. **f,** Severe fetal and placental growth restriction in *Igf2*^{UbKO} (*Igf2*$^{+/fl}$; *CMV*$^{Cre/+}$) mutants (n=3-8 litters at each developmental stage). **g,** Flow cytometry analysis shows that the majority (>80%) of *H19*-DMD^{EpiKO} (*Meox2*$^{+/Cre}$; *H19*-DMD$^{fl/+}$) mutant FPEC express YFP, demonstrating good efficiency of *Meox2*^{Cre} in these cells (n=9–15 per genotype). **h,** Fetal and placental overgrowth in *H19*-DMD^{EpiKO} mutants (n=3-4 litters at each

860 developmental stage). For all graphs, data is shown as averages or individual values ± SD. N.S. – non-
861 significant, * $P < 0.05$; ** $P < 0.01$; *** $P < 0.001$ calculated by two-way ANOVA plus Sidak's multiple
862 comparisons tests (**b**, **c**, **d**, **f**, **g**, **h**).

863

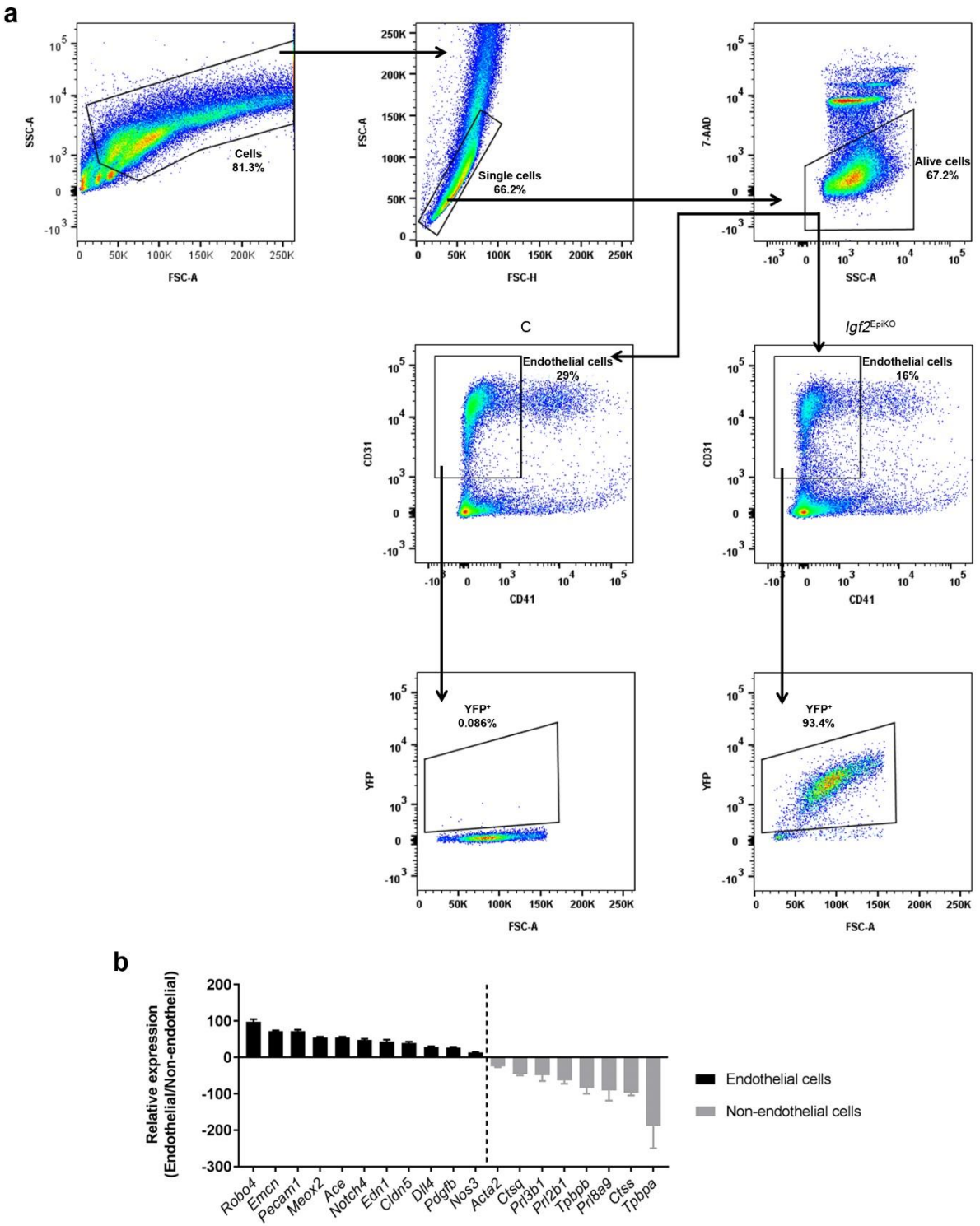

864

865

866 **Extended Data Figure 6: Experimental design used for FPEC analysis by flow cytometry and FPEC**
867 **isolation by FACS.**

868 **a,** Gating strategy used for flow cytometry analysis of FPEC and their isolation by FACS. FPEC are
869 defined as viable, single cells positive for CD31 and negative for CD41. Mutant FPEC are also positive
870 for YFP (activated by Cre mediated deletion of the *Rosa26* ^{fl}STOP^{fl}YFP STOP cassette), thus providing
871 an internal control for Cre efficiency in each biological sample. **b,** RNA-seq analysis of marker genes
872 expressed in FPEC or non-endothelial cells isolated by FACS from E16 control placental Lz. The graph
873 shows the relative enrichment in FPEC of known markers of endothelial cells (black) and depletion of
874 marker genes expressed by other cell types found in the placental Lz (grey): pericytes (*Acta2*),
875 sinusoidal trophoblast giant cells (*Ctsq*, *Prl2b1*, *Prl8a9*), parietal trophoblast giant cells (*Prl3b1*) or
876 spongiotrophoblast cells (*Tpbpa*, *Tpbpb*).

877

878

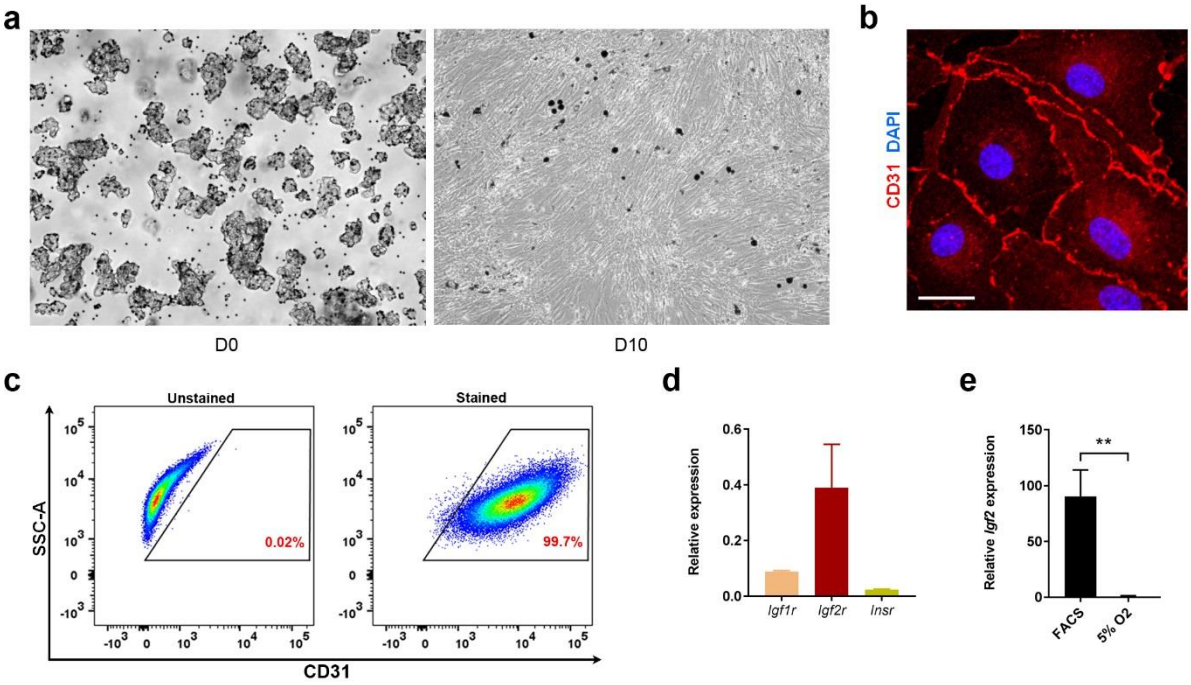

879

880

881 **Extended Data Figure 7: *Ex vivo* culture of primary FPEC isolated from E16 placental Lz.**

882 **a,** Primary FPEC isolated from E16 placental Lz: D0 – freshly isolated cells, bound to magnetic beads
883 coated with anti-CD31 antibodies; D10 – FPEC at passage one (after approximately 10 days of culture).
884 **b,** Confocal imaging of passage one FPEC, stained for CD31 (scale bar is 20 µm). **c,** Flow cytometry
885 analysis of passage one FPEC stained for CD31, demonstrating that these are almost exclusively CD31^{+}.
886 **d,** Relative expression of the three IGF receptors in passage one FPEC. **e,** qRT-PCR analysis of *Igf2*
887 mRNA levels in passage one FPEC cultured in 5% O2 versus primary FPEC isolated from E16 placental
888 Lz by FACS. For panels **d** and **e** data is presented as average values ± SEM (n=6 samples per group); **
889 $P < 0.01$ using a Mann Whitney test (**e**).

890

891

892

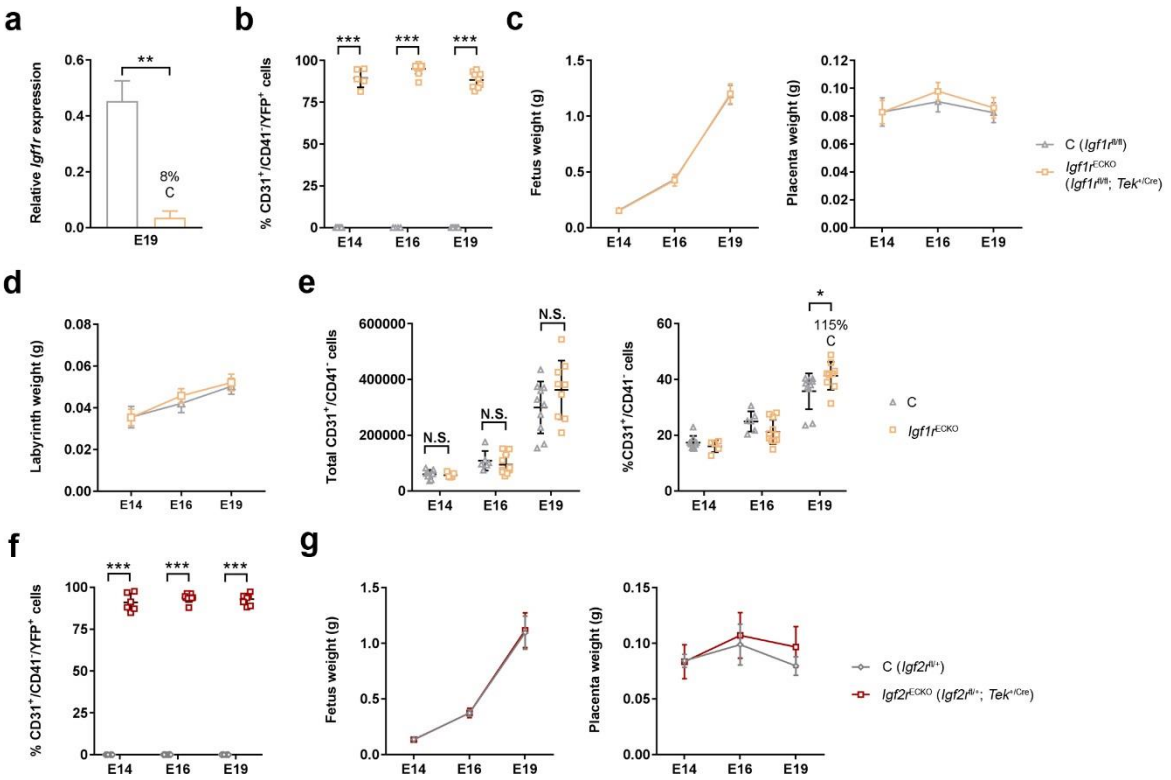

Extended Data Figure 8: Conditional deletions of *Igf1r and Igf2r* from endothelium using *Tek*^{Cre}.

a, qRT-PCR analysis of *Igf1r* mRNA levels in primary FPEC isolated by FACS from E19 placental Lz of *Igf1r*^{ECKO} (*Igf1r*$^{fl/fl}$; *Tek*$^{+/Cre}$) mutants versus *Igf1r*$^{fl/fl}$ controls. **b,** Flow cytometry analysis showing that the majority (>80%) of *Igf1r*^{ECKO} mutant FPEC express YFP, demonstrating good efficiency of *Tek2*^{Cre} in these samples (n=5–11 per genotype). Fetal, placental (**c**) and placental Lz (**d**) growth kinetics are not altered in *Igf1r*^{ECKO} mutants compared to controls (n=6–18 conceptuses from n=3-7 litters for each developmental stage). **e,** Total numbers and proportions of FPEC/placental Lz measured by flow cytometry (n=5–11 per genotype). **f,** Flow cytometry analysis showing that the majority (>80%) of *Igf2r*^{ECKO} mutant FPEC express YFP, demonstrating good efficiency of *Tek2*^{Cre} in these samples (n=6–14 per genotype). **g,** Fetal and placental growth kinetics are unaltered in *Igf2r*^{ECKO} (*Igf2r*$^{fl/+}$; *Tek*$^{+/Cre}$) mutants compared to *Igf2r*$^{fl/+}$ controls (n=8–28 conceptuses from n=3-8 litters for each developmental stage). For all graphs, data is shown as individual values or averages ± SD; N.S. – non-significant, * $P < 0.05$, ** $P < 0.01$, *** $P < 0.001$ by Mann-Whitney tests (**a**) or two-way ANOVA plus Sidak's multiple comparisons tests (**b** – **g**).

Supplementary Table 1: Top 100 highest expressed genes by RNA-Seq from FACS purified E16 feto-placental endothelial cells. FPKM values represent the average of n=4 independent biological replicates. Paternally expressed and maternally expressed imprinted gene symbols are coloured in blue and red, respectively.

Supplementary Table 2: List of differentially expressed genes identified through expression microarray analysis in placental Lz samples micro-dissected from E19 *Igf2*^{EpiKO} mutants (average of n=6) and controls (average of n=6). Upregulated and dowregulated gene symbols are coloured in blue and red, respectively.

918 **Supplementary Table 3**: List of differentially expressed genes by RNA-Seq from FACS purified feto-
919 placental endothelial cells of E16 *Igf2*^{EpiKO} mutants (average of n=4) and controls (average of n=4).
920 Upregulated and downregulated gene symbols are coloured in blue and red, respectively.

921

922 **Supplementary Table 4: Angiostatic and pro-angiogenic factors produced by feto-placental**
923 **endothelial cells under the control of fetus-derived IGF2**

Protein	Expression change	Function (cellular compartment)	Role in angiogenesis	PMID
CXCL10	Up-regulated	Cytokine (extracellular space)	angiostatic	7537965, 7540647, 8611715, 9064358, 10914483
IL15	Up-regulated	Cytokine (extracellular space)	angiostatic	28379958
THBS1	Up-regulated		angiostatic	22553494
ADAMTS1	Up-regulated	Peptidase (extracellular space)	angiostatic	12716911, 12814950, 17082774, 22776012
APCDD1	Up-regulated	Membrane-bound glycoprotein (cellular membrane)	angiostatic	29154126
IFIT2	Up-regulated	Interferon-induced protein (cytoplasm)	angiostatic	26515391
IFI16	Up-regulated	Transcription regulator (nucleus)	angiostatic	14729471, 21488755
CCL2	Up-regulated	Cytokine (extracellular space)	pro-angiogenic/ angiostatic if prolonged expression	15516694, 16888027, 23329645
EGR1	Up-regulated	Transcription regulator (nucleus)	pro-angiogenic/ angiostatic if prolonged expression	10339488, 12872165, 16818645, 27041221
KLF4	Up-regulated	Transcription regulator (nucleus)	pro-angiogenic/ angiostatic if prolonged expression	24599951, 27431648, 26823670
GDF15	Up-regulated	Growth factor (extracellular space)	pro-angiogenic	21773947, 28831101
HBEGF	Up-regulated	Growth factor (extracellular space)	pro-angiogenic	15289334, 18925469
SERPINE1	Up-regulated	Protease inhibitor (extracellular space)	pro-angiogenic	26180080
PLAT	Up-regulated	Peptidase (extracellular space)	pro-angiogenic	24601228
ISG20	Up-regulated	Exonuclease (nucleus)	pro-angiogenic	29195126
HEY2	Down-regulated	Transcription regulator (nucleus)	pro-angiogenic	15107403, 16219802, 22421041

924 **Supplementary Table 5: Primers used for genotyping by PCR**

Strain	Primer	Sequence	Primer	Sequence	Amplicon (bp)
Igf2$^{fl/fl}$	F	TTACAGTTCAAAGCCACCACG	RW RD	GCCAAAGAGATGAGAAGCACC GCCAAACACAGTAAAAAGAAATGC	WT: 324 fl: 449 del: 384
Rosa26 ^{fl}*STOP*^{fl}*YFP*	F	TGTTATCAGTAAGGGAGCT	R-WT R-fl	CACACCAGGTTAGCCTTTA AAGACCGCGAAGAGTTTGT	WT: 239 fl: 301
Meox2-Cre	F	GGACCACCTTCTTTTGGCTTC	R-WT R-Cre	AAGATGTGGAGAGTACGGGGTAG CAGATCCTCCTCAGAAATCAGC	WT: 410 Cre: 311
Tek-Cre	F	TGTAAACAAGAGCGAGTGGA	R-WT R-Cre	AGAGAATGGCGAGAAGTCAC TGAGTGAACGAACCTGGTCG	WT: 240 Cre: 610
Cyp19-Cre	F	GACCTTGCTGAGATTAGATC	R	AGAGAGAAGCATGTTTAGCTGG	Cre: 545
CMV-Cre	F	CGAGTGATGAGGTTCGCAAG	R	TGAGTGAACGAACCTGGTCG	Cre: 390
H19-DMD$^{fl/fl}$	F	CAGGCCTGTCCTCACCTGAAC	R	GCCAGCTTGCCTTGGCAACCCCTT	WT: 387 fl: 520
Igf2r$^{fl/fl}$	F	CCTTCCCTCCAGGCCGTTAC	R	GGTGAGGTCTCCATCTGAGTACC	WT: 225 fl: 259
Igf1r$^{fl/fl}$	F	CTTCCCAGCTTGCTACTCTAGG	R	CAGGCTTGCAATGAGACATGGG	WT: 124 fl: 220

925

926

927 **Supplementary Table 6: Conditions used for placenta immunostaining**

Staining	Antigen retrieval	Blocking	Primary antibody	Secondary antibody
IGF2	Digestion with 1% pronase (Protease from Streptomyces griseus, Sigma – P6911) in 1xPBS for 10 min at 37°C	15% Donkey serum (Sigma – D9663) in PBS	Goat anti-human IGF2 (1:50, R&D systems AF-292) overnight at 4°C	AF488 Donkey anti-goat (1:200, Jackson ImmunoResearch – 705-546-147), one hour at room temperature
YFP	Autoclaving for 15 min at 121°C in citric acid buffer (10 mM citric acid, pH 6.0, 0.05% Tween 20)	5% Donkey serum (Sigma – D9663) in PBS	Goat anti-GFP (1:200, Abcam – ab6673) overnight at 4°C	AF488 Donkey anti-goat (1:200, Jackson ImmunoResearch – 705-546-147), one hour at room temperature
CD31 (immune-histochemistry)	Boiling for 30 min in citric acid buffer (10 mM citric acid, pH 6.0, 0.05% Tween 20)	- 3% H2O2 solution (peroxidase inactivation) 30 min at room temperature; - 10% Goat serum (Sigma – G9023) and 1% BSA in PBS	Rabbit anti-CD31 (1:50, Abcam – ab28364) overnight at 4°C	Goat anti-Rabbit IgG, biotinylated (1:1000, Abcam – ab6720), one hour at room temperature, then Streptavidin-horse radish peroxidase (1:250 Rockland S000-03), one hour at room temperature, then DAB (Dako – K3468), 3-20 minutes at room temperature
CD31 (immune-	Boiling for 30 min in citric acid buffer (10 mM citric acid, pH	15% Donkey serum (Sigma – D9663) in PBS	Rabbit anti-CD31 (1:50, Abcam –	AF594 Donkey anti-rabbit (1:200, Jackson ImmunoResearch 711-

fluorescence – assay 1)	6.0, 0.05% Tween 20)		ab28364) overnight at 4°C	546-152), one hour at room temperature
CD31 (immune-fluorescence – assay 2)	Boiling for 20 min in Tris-EDTA buffer (10 mM Tris, 1 mM EDTA, 0.05% Tween 20, pH 9.0,)	Animal-free blocking solution (Vector – SP-5030)	Goat anti-CD31 (1:20, R&D – AF3628) overnight at 4°C	NL557-conjugated Donkey Anti-Goat (1:200, R&D – NL001), one hour at room temperature
F4/80	Heat-induced antigen retrieval in Target Retrieval Solution (pH=6) – Dako S236984-2	- Bloxall (peroxidase) Blocking Solution – Vector Labs SP-6000; - Animal-Free Blocker - Vector Labs SP-5030	Rat anti-Mouse F4/80 (1:20, [CI:A3-1] – Bio-Rad MCA497) 1 hour at room temperature	- Rabbit anti-Rat IgG (H+L) (1:250, Bethyl A110-322A) 1 hour at room temperature; - Anti-Rabbit HRP (ImmPress – Vector Labs MP-7451) 30 min at room temperature; - DAB (ImmPact DAB Kit - Vector Labs SK-4105)
MCT1	Proteinase K digestion (Dako – S3020) for 3 minutes at room temperature	15% Donkey serum (Sigma – D9663) in PBS	Chicken anti-MCT1 (1:200, Merk Millipore – AB1286-I) overnight at 4°C	AF488 Donkey anti-chicken (1:200, Jackson ImmunoResearch – 703-546-155), one hour at room temperature
MCT4	Proteinase K digestion (Dako – S3020) for 3 minutes at room temperature	15% Donkey serum (Sigma – D9663) in PBS	Rabbit anti-MCT4 (1:500, Merck Millipore – AB3314P) overnight at 4°C	AF488 Donkey anti-rabbit (1:200, Jackson ImmunoResearch – 711-546-152), one hour at room temperature
Laminin	Proteinase K digestion (Dako – S3020) for 3 minutes at room temperature	15% Donkey serum (Sigma – D9663) in PBS	Rabbit anti-laminin (1:500, Dako – Z0097) overnight at 4°C	AF488 Donkey anti-rabbit (1:200, Jackson ImmunoResearch – 711-546-152), one hour at room temperature

928

929

930 **Supplementary Table 7: Primers used for qRT-PCR**

Gene	Forward primer	Reverse primer	Amplicon (bp)
Igf2	AGTCCGAGAGGGACGTGTCTA	CGGACTGTCTCCAGGTGTCAT	102
Angpt1	GAAGCAACTTCTCAACAGACA	TTCTTTGTGTTTTCCCTCCATT	100
Angpt2	CTTCTACCTCGCTGGTGAAGAG	GCTAAAATCACTTCCTGGTTGG	106
Tek	GGAGTGGAGTGAAGAACTAGG	GTGGAGTCAGTGATGTTGGAGA	93
Adgre1	TAGCTGCTCTTCTGATACCCTC	CCAACATTCATCTTGTCCCCTC	145
Gcm1	CCGCAAGATTTACCTGAGACC	GAATAAGCTTCAGGGGTCCATT	98
Syna	AGCCCTCTCTGGACAATATTCA	CAAGGTGGGAGAAGATATTTGG	89
Synb	CAGCTGACACCCTCATTAAACA	ATCCAGAAATGGGAATGAAGTG	122
Slc16a1	TCGCAGCTTCTTTCTGTAACAC	TCATAGTCAGAGCTGGGTTCAA	102
Slc16a3	TGCAGAAGCATTATCCAGATCTAC	GTATCGATTGAGCATGATGAGG	99
Ly6e	ACATGAGAGTCTTCCTGCCTGT	TTCTGATCGGTACATGAGAAGC	91
Adamts1	CAAAGGACAGGTGCAAGCTC	TTGCACACAGACAGAGGTAGAG	119
Cxcl10	CGTCATTTTCTGCCTCATCCTG	TGATTTCAAGCTTCCCTATGGC	134
Thbs1	ATGTACCCATCCAGAGCATCTT	GGTTCCAAAGACAAACCTCACA	125
Edn1	GACATCATCTGGGTCAACACTC	AAGTCTTTCAAGGAACGCTTGG	86

Iigp1	ATGATTTGCCCTCCAGCTTTAC	ACTGAATATTCCCTTTTCTCATCCT	117
Cdkn1a	GAACATCTCAGGGCCGAAAAC	CACTTCAGGGTTTTCTCTTGCA	96
Hey2	CTGCCAAGTTAGAAAAGGCTGA	CTCATGAAGTCTGTGGCAAGAG	118
Igf1r	GTTATCCACGACGATGAGTGC	AGTCACCGAATCGATGGTTTTC	150
Igf2r	GGAAGACACCAGAACCAGACA	TGACACTCATCCTCTGGAAGC	103
Insr	GAGAGGATGTGAGACGACGG	AGCAGTTCTCCAGCTCATGTAG	149
Gapdh	ACAACTCACTCAAGATTGTCAGCA	ATGGCATGGACTGTGGTCAT	121
Sdha	TTCCGTGTGGGGAGTGTATTG	ATTCTGCAGCTCCAGGGTCTC	135
Pmm1	ATCCGGGAGAAGTTTGTGGAA	GCTGTCTTCATCCAGGCTGTC	144
Ppia	AAGGGTTCCTCCTTTCACAGAA	GATGCCAGGACCTGTATGCTT	146